**KIT**

Karlsruhe Institute of Technology

**Institute for Theoretical Physics**

# Aspects of Hadron Production in Herwig

Master's Thesis of

## Ronja Zimmermann

at the Department of Physics
Institute for Theoretical Physics (ITP)

Reviewer:            PD. Dr. S. Gieseke
Second reviewer:   Prof. Dr. G. Heinrich

31. Juli 2020 – 02. August 2021

I declare that I have developed and written the enclosed thesis completely by myself, and have not used sources or means without declaration in the text.

**PLACE, DATE**

. . . . . . . . . . . . . . . . . . . . . . . . . . . . . . . . . . .

(Ronja Zimmermann)

# Abstract

Large parts of the simulation of particle collisions take place in a low-energy regime and thus, rely on phenomenological models. The hadronization process describing the transition from partons to colour-neutral hadrons is one of these soft parts. The Monte Carlo event generator *Herwig* makes use of the cluster hadronization model. An important step of this is colour reconnection, in which the predefined colour structure from the parton shower is allowed to change. In the first part of this thesis, a new colour reconnection model is implemented and analysed. The novelty is that for the first time clusters with baryonic quantum numbers are included in the reconnection process. In the second part, the description of angular-correlations of identified particles is studied. In order to improve the description of these observables, another new model aiming to decorrelate the particles evolving from the hadronization is incorporated into Herwig. The model is analysed and its results are discussed.

# Zusammenfassung

Große Teile der Simulation von Teilchenkollisionen finden bei niedrigen Energien statt und beruhen daher auf phänomenologischen Modellen. Der Hadronisierungsprozess, der den Übergang von Partonen zu farbneutralen Hadronen beschreibt, ist einer dieser nicht störungstheoretischen Elemente. Der Monte Carlo Event Generator *Herwig* verwendet hierfür das sogenannte Cluster-Hadronisierungsmodell. Ein wichtiger Teil von diesem ist die sogenannte *Colour Reconnection*, bei der die aus dem Partonenschauer vorgegebene Farbstruktur geändert wird. Im ersten Teil dieser Arbeit wird ein neues Colour Reconnection Modell implementiert und analysiert. Die Besonderheit von diesem besteht darin, dass zum ersten Mal Cluster mit baryonischen Quantenzahlen in den Reconnection-Prozess integriert werden. Im zweiten Teil wird die Beschreibung von Korrelationen bezüglich des azimutalen Winkels von Teilchenpaaren im Endzustand betrachtet. Um die Beschreibung dieser Observablen zu verbessern, wird ein neues Modell zur Dekorrelation der Teilchen nach dem Hadronisierungsprozess in Herwig eingearbeitet. Das Modell wird analysiert und die aus ihm resultierenden Ergebnisse werden diskutiert.

# Contents

# 1. Introduction

Modern particle physics strives towards a fundamental understanding of the Universe and the inherent laws of Nature. For this purpose, the study of particle behaviour at high energies - as a method to probe the structure and physics of the early stages of the Universe - is indispensable. This is why many high-energy particle colliders have been built over the last century. A prominent and current example is the Large Hadron Collider (LHC). There, in 2012, the Higgs Boson was discovered, which was the last missing piece of the Standard Model (SM) of particle physics. However, there are phenomena that are not described by the Standard Model and therefore, are not fully understood so far, for instance, the matter–antimatter asymmetry in the Universe as well as the nature of dark matter and dark energy. One main goal of current and future experiments is the investigation of physics Beyond the Standard Model (BSM). For this task, an ongoing improvement of theoretical predictions and the understanding of the various aspects of particle collisions is crucial.

In this respect, simulation has become increasingly important. Simulation translates theoretical models into observables and thus, enables the comparison of theoretical predictions and experimental data. An important example for simulation software are Monte Carlo event generators, which use Monte Carlo methods for numerical integration.

To a certain extent, the simulation relies on perturbative calculations which can be carried out in high precision. However, perturbation theory is only valid in a high-energy regime. Large parts of the event generation lie outside this regime and depend on phenomenological models which are not fully described by a theoretical model, instead relying on experimental observations and theoretical considerations. Examples include the hadronization process, which describes the transition from colour-charged partons to colour-neutral hadrons, and parts of the underlying event.

In order to simulate an event that is as exclusive as possible, it is indispensable that not only the high-energy parts of the event are simulated accurately, but also the so-called soft parts. For the sake of validating the simulation process, its output is compared to data from former experiments. Data measured with a minimum bias trigger are rigourous arenas for testing soft models.

Within the framework of this thesis, the Monte Carlo event generator *Herwig* [1−4] is extended by two new phenomenological models.

In the first part, we introduce a new colour reconnection model. Colour reconnection is an important part of the hadronization process, which allows different parts of the event, i.e. the hard process and the underlying event, to interfere with each other. It is crucial for the accurate description of various observables. The new model is compatible with the current version of Herwig and can be seen as an alternative to the three different colour reconnections models Herwig already provides.

In the second part, the description of angular-correlation of identified particles is exam-

ined. These angular-correlations are minimum bias observables, which have never been considered in detail for the Herwig cluster model. We will see that in some parts Herwig fails to describe these observables accurately and suggest and investigate the reasons for that. Through the gained insights, a new model is motivated and implemented into Herwig, in order to obtain an improvement in the description of this data.

This thesis is structured as follows: Since we focus on hadron collisions and aspects affecting colour-charged particles, chapter 2 gives a short introduction to quantum chromodynamics (QCD), which describes the interaction of colour-charged particles. Subsequently, chapter 3 explains the individual steps of the event simulation with Herwig and can be seen as a short introduction to Monte Carlo event generators. Chapter 4 deals with the motivation, implementation and analysis of the new colour reconnection model, namely the *baryonic-mesonic colour reconnection model*. In chapter 5 the angular-correlation observables are discussed and subsequently, the *post-hadronization momentum swapping model* is introduced and analysed. Finally we summarize the work and perceptions of this thesis and give a brief outlook in chapter 6.

# 2. Quantum Chromodynamics

In particle physics the Standard Model (SM) describes the fundamental particles and their interactions. The SM combines the electroweak theory and *quantum chromodynamics* (QCD), which are both quantum field theories. The following is a brief introduction to QCD with focus on the parts which are relevant for simulation of hadron collisions in general and the work of this thesis in particular. For a more detailed description of QCD the interested reader is referred to the various textbooks on this topic, e.g. [5].

QCD describes the interactions among colour-charged particles, such as quarks and gluons, which is referred to as the *strong interaction* and is one of the four fundamental forces in the Universe. In QCD quarks are massive spin-1/2 particles, whereas gluons are massless bosons with spin 1. Quarks and gluons are conventionally referred to as partons, a name that originates from Feynman's original parton model of the strong force [6].

In Nature no single colour-charged particles are observed but only particles which are neutral in colour-charge, so-called colour-singlets. These composite particles consist of partons and are referred to collectively as hadrons. Hence, there is a need for a description of the transition from the parton-level interactions in hard processes to the colourless hadrons that are detected. The formation of hadrons, which is referred to as *hadronization*, happens at energy scale of $O(1 \text{ GeV})$. While at higher energy, where the partons are approximately free, the interaction can be calculated in perturbation theory, this approach is not valid for lower energies. Thus, the description of hadronization processes relies on phenomenological models.

## 2.1. QCD Lagrangian

QCD is a $SU(3)_C$ non-abelian gauge theory. It is described by its Lagrangian density,

$$\mathcal{L} = -\frac{1}{4}F^a_{\mu\nu}F^{\mu\nu}_a + \sum_{q=\text{flavours}} \bar{\Psi}_{q,i}(i\gamma^\mu D_\mu - m_q)_{ij}\Psi_{q,j} + \mathcal{L}_{\text{gauge}} + \mathcal{L}_{\text{ghost}}, \tag{2.1}$$

where $F^a_{\mu\nu}$ is the field strength tensor determined by the eight massless gluon fields $A^a_\mu$, that correspond to the eight $SU(3)_C$ generators $T^a$:

$$F^a_{\mu\nu} = \partial_\mu A^a_\nu - \partial_\nu A^a_\mu - g_s f^{abc} A^b_\mu A^c_\nu, \tag{2.2}$$

where $g_s$ is the strong coupling constant, $a$, $b$ and $c$ the colour indices and $f^{abc}$ is the structure constant of $SU(3)_C$, which is determined by the commutation relation of the

generators:

$$[T^a, T^b] = i f^{abc} T^c. \tag{2.3}$$

In the fundamental representation the generators are $T^a = \frac{\lambda_a}{2}$, where $\lambda_a$ refer to the Gell-Mann matrices.

The second term of equation 2.1 corresponds to the kinetic energy of the quarks and their interaction with the gluons, which leaves the flavour of the quarks unchanged. Here $\Psi_q$ is the spinor corresponding to the quark field with flavour $q$ and mass $m_q$. $D_\mu$ is the covariant derivative, which is given by:

$$D_\mu = \partial_\mu - i g_s T^a A_\mu^a. \tag{2.4}$$

$\mathcal{L}_{\text{gauge}}$ is a gauge-fixing term, which leads to a particular gauge choice. This is required, among other things, to define the gluon propagator properly. There are some degrees of freedom in choosing the gauge-fixing term. A common gauge, for instance, is the *covariant gauge*, that leads to unphysical degrees of freedom, which have to be cancelled. This is done via the ghost term $\mathcal{L}_{\text{ghost}}$ which is a complex scalar field and entails an additional ghost propagator and vertices. However, the *axial gauge* is defined in such a way that the ghost-term vanishes.

## 2.2. Asymptotic Freedom and Confinement

The fundamental picture of QCD consists of colour-charged particles interacting with coupling strength $\alpha_S = \frac{g_s^2}{4\pi}$. However, technically the coupling constant $\alpha_S$ is not a constant, since it depends on the momentum transferred in the interaction. It is often referred to as *running coupling constant.*

In *renormalization theory* - where divergent parts of the expansion in $\alpha_S$ in perturbative calculations are cut off - the scale-dependence of the coupling is expressed through the *renormalization group equation* [5],

$$\beta(\alpha_S) = Q^2 \frac{\partial \alpha_S}{\partial Q^2}, \tag{2.5}$$

where $Q$ is the scale of the momentum transfer in the interaction. In equation 2.5 $\beta$ can be written in terms of the strong coupling $\alpha_S$,

$$\beta(\alpha_s) = -(b_1 \alpha_S^2 + b_2 \alpha_S^3 + O(\alpha_S^4)) \tag{2.6}$$

with the coefficients

$$b_1 = \frac{33 - 2n_f}{12\pi} \qquad b_2 = \frac{153 - 19n_f}{24\pi^2}. \tag{2.7}$$

Here $n_f$ is the number of active quark flavours. In QCD $n_f \leq 6$ is true in general. For $n_f \leq 16$ the coefficients have negative signs. Thus, in QCD for asymptotically high energies, i.e. small distances, the coupling vanishes. This phenomenon is called *asymptotic freedom* [7] [8] and entails that at large energies partons asymptotically behave as if they were free particles.

If the expansion of $\beta(\alpha_S)$ (equation 2.6) is truncated after the term quadratic in $\alpha_S$, which is reasonable in the perturbative regime ($Q^2, \mu_R^2 \gg 1 \text{ GeV}^2$), the solution for equation 2.5 is given by

$$\alpha_S(Q^2) = \frac{\alpha_S(\mu_R^2)}{1 + \alpha_S(\mu_R^2) \cdot b_1 \cdot \ln\left(\frac{Q^2}{\mu_R^2}\right)}. \tag{2.8}$$

Here it should be pointed out that as $\ln\left(Q^2/\mu_R^2\right)$ becomes large $\alpha_S$ approaches 0. Thus, asymptotic freedom for large energy scales $Q^2$ can be directly read from this equation. Equation 2.8 describes the energy-dependent behaviour of the coupling $\alpha_S$. That means if $\alpha_S(\mu_R^2)$ is known for a certain energy scale $\mu_R^2$, the coupling $\alpha_S(Q^2)$ at any other scale $Q^2$ can be deduced by using equation 2.8. However, the coupling has to be measured. A plot of current measurements on $\alpha_S$ at different energy scales is shown in figure 2.1. A common scale for $\alpha_S$-measurements is, for instance, the pole of the Z-Boson mass, $M_Z = 91.2 \text{ GeV}$. At this scale the coupling has been measured to be $\alpha_S \approx 0.118$.

For this reference scale the running coupling exceeds the value 1 for $Q^2 < \mathcal{O}(1 \text{ GeV}^2)$. At this energy regime the truncated equation for $\beta(\alpha_S)$ is not valid, since the contribution of terms in $\alpha_S$ increases with higher orders. Hence, perturbation theory is not longer valid. An alternative approach is introducing a dimensional parameter $\Lambda_{QCD}$ which sets the scale at which $\alpha_S$ diverges. The energy behaviour of the running coupling then reads

$$\alpha_S(Q^2) = \frac{1}{b_1 \ln\left(\frac{Q^2}{\Lambda_{QCD}^2}\right)}. \tag{2.9}$$

$\Lambda_{QCD}^2$ depends on the used renormalisation scheme and also the order up to which the $\beta(\alpha_S)$ function is considered. As already implicitly mentioned the coupling diverges, when $Q^2$ approaches $\Lambda_{QCD}^2$. This corresponds to the so-called *confinement* property of QCD, which implies that all colour-charged particles form colour-neutral states at energy scale $\mathcal{O}(1 \text{ GeV})$. Thus, perturbation theory breaks down and no single partons are observed at macroscopic scales.
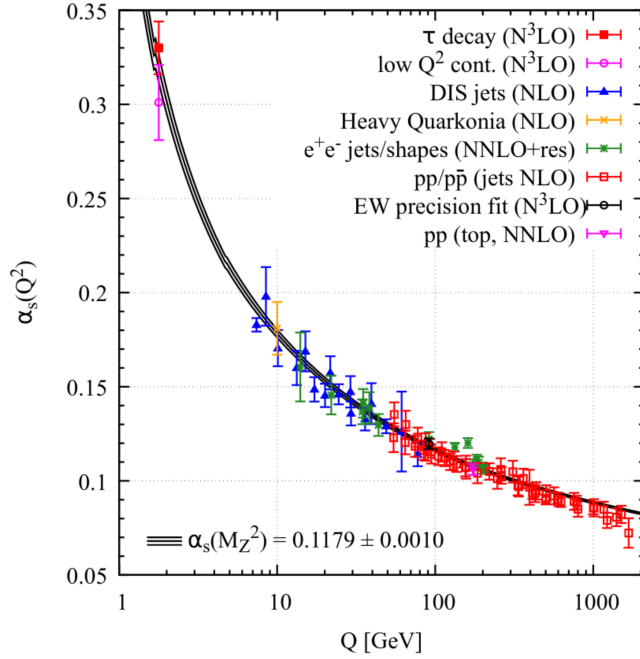
Figure 2.1.: The strong coupling contant $\alpha_S(Q^2)$ plot taken from [9]. Shown is $\alpha_s(Q^2)$ of several measurements as a function of the energy scale $Q^2$. The solid lines show the predicted behaviour of $\alpha_S(Q^2)$ extrapolated from the measured value of the coupling $\alpha_S(M_Z^2)$ at the Z-pole $M_Z$. The plot illustrates the energy-dependent behaviour of the $\alpha_S(Q^2)$. For small energy it diverges towards confinement, while for high energy it decreases.

### 2.2.1. Colour Flow and large-$N_C$ Limit

In QCD the colour structure of each Feynman rule and thus, of each Feynman diagram can be decomposed into Kronecker-deltas $\delta_{ij}$ between external colours. This is called the *colour flow* of the diagram and shows how the colour evolves during an interaction. Consider the example of the quark-gluon vertex given by the Feynman rule:

$$-ig_s\gamma^a T_{ij}^a. \tag{2.10}$$

So its matrix element contains the square of the generator $T_{ij}^a$. Using the Fierz identity one can show that

$$T_{ij}^a T_{kl}^a = \frac{1}{2}\left(\delta_{il}\delta_{jk} - \frac{1}{N_c}\delta_{ij}\delta_{kl}\right). \tag{2.11}$$

The two terms correspond to two Feynman diagrams with different colour flows. They are shown in figure 2.2. For the first term the colour flow can be seen as going between the quarks and the gluon, while for the second term the colour flows between the quarks, and the gluon carries a colour and the same anticolour, the so-called colour-singlet gluon. The contribution of the second diagram is suppressed by a factor of $\frac{1}{N_C}$. Hence, it decreases for

higher numbers of colour-charges. In the $N_C \rightarrow \infty$ limit [10], where an arbitrary number of colours is supposed, it vanishes completely and thus,

$$T_{ij}^a T_{kl}^a \approx \frac{1}{2} \delta_{il} \delta_{jk}.$$ (2.12)

Therefore, in this limit only the first diagram contributes. Similar considerations can be done for the 3-gluon-vertex and the 4-gluon-vertex. In general it can be shown that in the $N \rightarrow \infty$ limit gluons are always part of two different colour lines and thus, the colour structure is planar. This limit is quiet powerful and crucial for Monte Carlo event generation. In Herwig, for instance, the hadronization model (see section 3.3) is based on it.



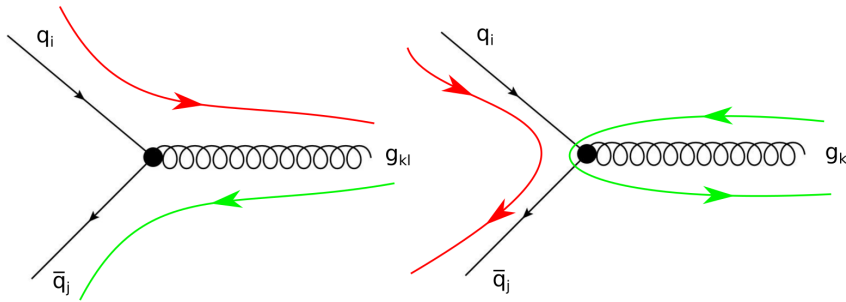Figure 2.2.: The two contributing Feynman diagrams for the quark-gluon vertex with different colour flow. On the left-hand side the leading diagram with a colour line between the quark and the gluon, and an anticolour line between the gluon and the antiquark. On the right-hand side the subleading diagram is suppressed by a factor of $\frac{1}{N_C}$, where the colour flow is within the gluon and between the quark and the antiquark.

# 3. Monte Carlo Event Generation with Herwig

General-purpose Monte Carlo event generators like *Herwig* [1–4] are used to simulate particle collisions at high energies, such as those taking place at collider experiments, for example at the LHC [11]. To get a good description of data it is imperative to accurately simulate all aspects of the process, from the first particle collisions to the transition to the finale particle states, as measured in the detector. Thus, the simulation contains a number of different physical processes separated in energy scales. Processes happening at a characteristic energy scale above the hadronization scale are governed by perturbation theory, while those below it rely on non-perturbative phenomenological models.

The main steps of the simulation are the hard scattering process, the parton shower and the hadronization process. To simulate the underlying event, additional semi-hard and soft interactions between the remnants of the colliding particles occur in hadron-hadron collisions. In figure 3.1 a schematic overview of a simulated proton-proton collision without the underlying event is illustrated. During the hard process two incoming particles scatter at a high-energy scale calculated in perturbative theory by summing over all Feynman diagrams of the relevant process up to a certain order of the coupling constants. The outgoing particles radiate perturbatively in the parton shower by emitting particles until they reach an energy scale close to the hadronic scale, where perturbation theory is no longer valid. In addition, the outgoing particles of the semi-hard underlying-event processes shower to this soft regime.

After the parton shower the hadronization takes place, where the partons originating from the hard process, the semi-hard and soft underlying-event processes and also the hadron-remnants form colour-singlet particles. This is done in the soft-regime of event simulation. In Herwig the so-called *cluster hadronization model* is implemented. Colour-connected particle pairs form colour-neutral clusters and decay together in two excited particle states. These excited states finally decay into the final state particles measured in the detector. In the following the individual steps of the event simulation are discussed in detail.
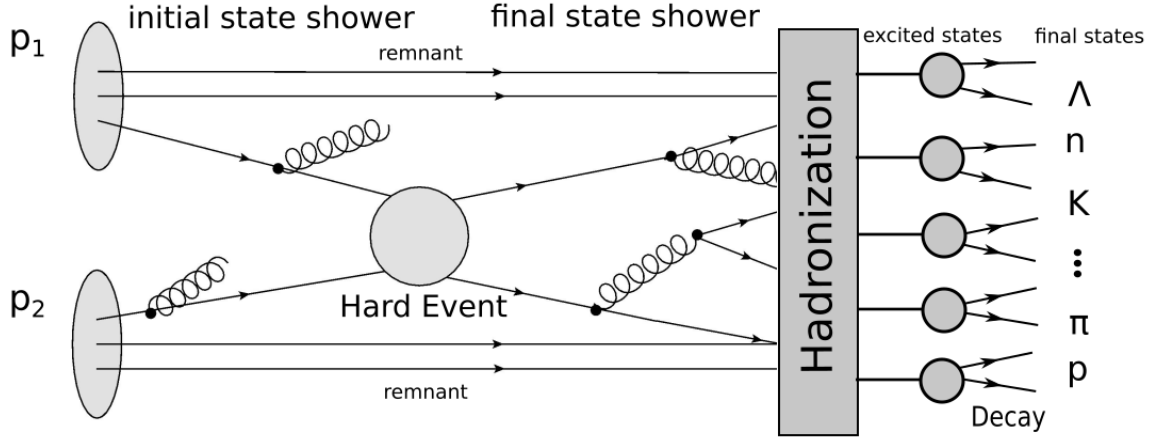
Figure 3.1.: Schematic overview of the event generation process. The core of the event is the hard process. Through the parton shower the primary outgoing particles lower their energy down to the hadronic scale by emitting partons. The hadronization then describes the formation of excited hadrons, which finally decay into the finale state particles measured in the detector.

## 3.1. Hard Scattering Process

One of the major elements of event simulation is the hard scattering process, in which the incoming particles collide. These processes involve large transverse momentum transfer. For the determination of the cross section, the species of the incoming particles are important. In lepton collisions the involved particles are elementary and thus, calculating the cross section is relatively straight forward. In contrast, hadrons are composite particles and therefore, their exact composition and inner momentum structure have to be taken into account.

The cross section for $ij \rightarrow n$ hadron scattering is given by [5]:

$$\sigma = \sum_{i,j} \int_0^1 dx_1 \, dx_2 \, f_i(x_1, \mu_F) f_j(x_2, \mu_F) \times \hat{\sigma}(p_i, p_j, \alpha_s(\mu_F), Q^2/\mu_F) \qquad (3.1)$$

Where $f_i(x, \mu_F)$ is the parton distribution function (PDF), which at leading order gives the probability for finding a parton $i$ with the momentum fraction $x$ of the total hadron momentum at energy scale $\mu_F$.

$\hat{\sigma}(p_i, p_j, \alpha_s(\mu_F), Q^2/\mu_F)$ is the cross section for a two parton collision and is given by:

$$\hat{\sigma}(p_i, p_j, \alpha_s(\mu_F), Q^2/\mu_F) = \int d\Phi_n \, \frac{1}{2s} |\mathcal{M}_{ij \rightarrow n}|^2 (\Phi_n; \mu_F, \mu_R), \qquad (3.2)$$

where $|\mathcal{M}_{ij \rightarrow n}|^2$ is the squared matrix element, which represents all possible processes in the hard scattering process as a sum of Feynman diagrams. In addition $\frac{1}{2s}$ denotes the parton flux and $d\Phi_n$ is the differential phase space element for a final state with $n$ particles.

Determining the hard process relies heavily on the choice of matrix elements and PDFs. In Herwig 7 the considered processes can be set by the user. Herwig provides a limited number of built-in matrix elements, but also additional matrix elements can be accessed by using the external matrix element providers GoSam [12, 13], OpenLoops [14], VBFNLO [15–17] and MADGRAPH [18].

Moreover Herwig provides built-in PDFs, but also additional PDFs are available using LHAPDF [19].

The particles of the hard scattering process are forwarded to the parton shower, where they undergo perturbative stochastic radiation.

## 3.2. Parton Shower

In Herwig the hard scattering process is calculated up to next-to-leading order (NLO) of the strong coupling constant ($\alpha_s$). But beyond that level the complexity of determining the matrix elements grows. Thus, it would take too much computing power to do further calculations.

However, higher order corrections are not negligible in all regions of phase space. Due to this, an additional approach is required to include these corrections.

The parton shower implemented in Herwig is such an approach. Starting at the energy of the hard scattering process ($Q^2$), it evolves particles by quark and gluon radiation down to the hadronic scale $Q_0^2 \approx 1$ GeV at which confinement is valid and partons form hadrons.

In Herwig two different approaches of the parton shower are available. The so-called *angular-ordered shower*, which is set as default, and the *dipole shower*, which can be chosen as an alternative.

The section is structured as follows: First, the basic idea and theoretical background of the final- and initial-state parton shower [20] is introduced. Subsequently, the two different parton shower algorithms implemented in Herwig are discussed in more detail.

### 3.2.1. Final State Shower

To illustrate the basic features of the parton shower, consider the process $e^+e^-$ to two jets. Later we will generalize these points to a process-independent approach.

For the process $e^+e^- \rightarrow q\bar{q}$ the total cross section in leading order $\sigma_{q\bar{q}}$ can be calculated in perturbative theory. In the next to leading order process one of the quarks emits an additional gluon: $e^+e^- \rightarrow q\bar{q}g$. Its differential cross section is given by:

$$\frac{d\sigma_{q\bar{q}g}}{d\cos\theta\, dz} \approx \sigma_{q\bar{q}} \cdot C_F \frac{\alpha_s}{2\pi} \frac{2}{\sin^2\theta} \frac{1+(1-z)^2}{z}. \tag{3.3}$$

Here $z$ is the energy fraction of the gluon, $\theta$ the opening angle between the gluon and the quark. $C_F$ is a colour factor depending on the number of colour charges. It can be easily seen that the total cross section $\sigma_{q\bar{q}g}$ is proportional to the leading order cross section $\sigma_{q\bar{q}}$. Hence, the rest of the equation can be interpreted as the probability that an additional gluon is emitted.

In equation 3.3 two types of divergence appear: The first occurs at $\theta \to 0$ and $\theta \to \pi$ corresponding to the emitted gluon becoming collinear to the quark or anti-quark respectively. Additionally, the second type occurs as $z \to 0$. This is referred to as soft divergence and corresponds to the gluon energy going towards zero.

First, consider the collinear divergences. The term responsible for the divergences can be split in two:

$$\frac{2}{\sin^2 \theta} = \frac{1}{1 - \cos \theta} + \frac{1}{1 + \cos \theta} \approx \frac{1}{1 - \cos \theta} + \frac{1}{1 - \cos \bar{\theta}}. \tag{3.4}$$

Here $\bar{\theta}$ represents the angle between the gluon and the anti-quark. The last approximation is only valid in the limit $\theta \to 0$ or $\theta \to \pi$ respectively. Using this expression in the mentioned limit equation 3.3 can be rewritten as follows:

$$d\sigma_{q\bar{q}g} \approx \sigma_{q\bar{q}} \cdot \sum_{q\bar{q}} C_F \frac{\alpha_s}{2\pi} \frac{d\theta^2}{\theta^2} \, dz \frac{1 + (1 - z)^2}{z} \tag{3.5}$$

Hence, the differential cross section is expressed as the sum of independent emissions of the two partons. In equation 3.5 $\theta$ is the opening angle between the gluon and the respective parton. For other phase space parametrisations with variables that are proportional to $\theta$, like the virtuality of the off-shell quark propagator $q^2$ or the transverse momentum of the gluon $k^2$, mathematically-identical expressions are obtained.

It can be shown that the structure of equation 3.5 is completely generalizable. Thus, the differential cross section for any hard process with an additional parton $j$ with momentum fraction $z$ can be expressed by:

$$d\sigma \approx \sigma_0 \cdot \sum_i \frac{\alpha_s}{2\pi} \frac{d\theta^2}{\theta^2} \, dz P_{ji}(z, \phi) \, d\phi. \tag{3.6}$$

Here $\sigma_0$ is the cross section for the process without the additional parton. $P_{ji}(z, \phi)$ are the so-called *DGLAP splitting functions* [21, 22], which depend on flavour and in general also on spin. Averaged over spin they are given by:

$$P_{qq}(z) = C_F \frac{1 + z^2}{1 - z}, \tag{3.7}$$

$$P_{gq}(z) = C_F \frac{1 + (1 - z)^2}{z}, \tag{3.8}$$

$$P_{gg}(z) = C_A \frac{z^4 + 1 + (1 - z)^4}{z(1 - z)}, \tag{3.9}$$

$$P_{qg}(z) = T_R \cdot (z^2 + (1 - z)^2), \tag{3.10}$$

where $C_F$, $C_A$ and $T_R$ are again colour factors. $P_{qq}$, $P_{gq}$, $P_{gg}$ and $P_{qg}$ correspond respectively to the splittings $q \to qg$, $q \to gq$, $g \to gg$ and $g \to q\bar{q}$.

Now an iterative algorithm can be derived by utilizing expression 3.6. First, it is applied to the hard process to induce a splitting and emit an additional parton. In a next step, it is applied to the resulting products to generate more splittings.

At this point, the divergences are not taken into account. Partons that are exactly collinear and have the same quantum numbers are physical indistinguishable. Therefore, it is reasonable to only produce resolvable partons which fulfil a resolution criteria. For instance, the transverse momentum can be used as such a criteria. Two partons are referred to as resolvable, if their relative transverse momentum is above a cut-off scale $Q_0^2$. In that way collinear and soft divergences are guarded, since singularities are cancelled between virtual and unresolved terms.

Up to now, the calculated distribution is the inclusive distribution of all gluon emissions. In order to get the distribution of multiple gluon events and thus, describe multiple branchings, the distributions of individual gluons have to be separated out. For that the virtuality of the inner quark propagator $q^2$ is used as an ordering variable. The distribution calculated before can then be regarded as the probability for the emission of a parton of type $i$ in the energy range $q^2$ and $q^2 + dq^2$:

$$d\mathscr{P} = \frac{\alpha_s}{2\pi} \frac{dq^2}{q^2} \int_{\frac{Q_0^2}{q^2}}^{1-\frac{Q_0^2}{q^2}} dz P_{ji}(z). \tag{3.11}$$

The limits on $z$ follow from the resolution conditions. To determine the probability of the first branching at $q^2$, the probability that no branching at a scale higher than $q^2$ happened $\Delta_i(q^2, Q_0^2)$ is used. $\Delta_i(q^2, Q_0^2)$ is called the Sudakov form factor and is defined by:

$$\frac{d\Delta_i(q^2, Q_0^2)}{dq^2} = \Delta_i(q^2, Q_0^2) \frac{d\mathscr{P}}{dq^2}. \tag{3.12}$$

It can be shown that the solution of this differential equation and so the Sudakov form factor is given by:

$$\Delta_i(q^2, Q_0^2) = \exp\left\{ -\int_{Q_0^2}^{Q^2} \frac{dk^2}{k^2} \frac{\alpha_s}{2\pi} \int_{\frac{Q_0^2}{q^2}}^{1-\frac{Q_0^2}{q^2}} dz P_{ji}(z) \right\}. \tag{3.13}$$

$Q^2$ is the maximal possible virtuality. The Sudakov form factor can be used to implement a Monte Carlo shower by using it to determine the scale $q'^2$ for the next branching. This can be done, for instance, by generating a random number $R$ in the interval $[0,1]$ and subsequently solving the equation

$$R = \Delta_i(Q^2, q'^2). \tag{3.14}$$

If the calculated solution for $q'^2$ is greater than the cut-off scale $Q_0^2$, a branching at the scale $q'^2$ is generated. The value for $z$ is determined according to the splitting function $P_{ij}(z)$. This procedure is repeated recursively for each branching product until $q'^2 < Q_0^2$, which means that the calculated branching would not be resolvable.

## 3.2.2. Initial State Shower

So far, only the showering of particles produced in the hard process were considered. As one would expect, the incoming particles before the actual collision are able to perform a shower as well. The forward showering described in the previous section could be applied on the incoming particles. However, that would be fairly inefficient, since partons with the correct kinematics for the requested hard process are required.

Therefore, in Monte Carlo event generators usually the hard process is the starting point around which additional initial and final radiation is simulated. That means, the initial-state shower is generated backwards from the hard process to the incoming protons.

The Sudakov form factor of equation 3.13 is replaced by one depending on the PDFs of the colliding hadrons:

$$\Delta_i(Q^2, q^2, x) = \exp\left\{ -\int_{q^2}^{Q^2} \frac{dk^2}{k^2} \frac{\alpha_s}{2\pi} \int_{\frac{Q_0^2}{k^2}}^{1-\frac{Q_0^2}{k^2}} dz P_{ji}(z) \frac{\frac{x}{z} \cdot f_j(\frac{x}{z}, k^2)}{x \cdot f_i(x, k^2)} \right\}, \qquad (3.15)$$

where $x$ is the initial momentum fraction of the parton while contributing to the hard process and $\frac{x}{k}$ is its moment fraction at the stage to which it possibly evolves back.

Due to the PDF-ratio it is very likely that the shower terminates at the stage of a valence quark, because their PDF are dominant for high-$x$. However, in cases where this does not happen by itself, the termination at the stage of a valence quark is forced by performing additional branchings.

The partons emitted by the initial state shower will perform additional final state showers.

## 3.2.3. Parton Shower Algorithms

The default shower algorithm in Herwig 7 is the angular-ordered shower [23]. The user can also choose the so-called dipole shower algorithm [24, 25]. Both are briefly discussed below.

### 3.2.3.1. Angular-ordered Shower

The angular-ordered shower in Herwig 7 is based on the coherent branching algorithm, which provides angular ordering conservation and invariance under boosts along the jet axis. For a detailed derivation the interested reader is referred to [23]. Here only the key-elements are pointed out briefly.

The evolution scale $\tilde{q}^2$ for the branching $a \rightarrow bc$ with parent $a$ and children $b$ and $c$ in

terms of the respective opening angles is given by:

$$\tilde{q}^2 = \frac{2E_a(1 - \cos\theta_{bc})(1 + \cos\theta_a)^2}{(1 + \cos\theta_b)(1 + \cos\theta_c)},$$ (3.16)

where $\theta_{bc}$ denotes the angle between the children and $\theta_a$, $\theta_b$ and $\theta_c$ denote the opening angle between the respective parton and the so-called shower progenitor. Shower progenitors are the partons from the hard process initiating the shower. $E_a$ is the energy of the parent. For small emission angles equation 3.16 can be approximated as

$$\tilde{q} = E_a\theta_{bc}.$$ (3.17)

The child-partons have momentum fraction $z$ and due to four-momentum conservation $(1 - z)$. Angular ordering is then ensured by setting the maximum evolution scale for the branching to $z\tilde{q}$ and $(1 - z)\tilde{q}$ respectively. Hence, the maximum opening angle of a subsequent branching is less than or equal to $\theta_{bc}$.

As long as only quarks are involved in a branching its colour flow is unique. For gluons there are two possible configurations of the colour lines, either their colour line or their anticolour line breaks up for emission. In this case a random choice is made.

### 3.2.3.2. Dipole Shower

In the limit of a $N_c \to \infty$ [10], where $N_c$ denotes the number of colour-charges, the colour structure of the parton shower is such that it can be drawn on a plane and is composed in colour lines. Each colour line links a colour-charged parton with an anticolour-charged parton and thus, can be seen as colour-anticolour dipole. The generation of the shower then takes place through radiations of these dipoles and the resulting emissions, which are independent of each other in the considered limit $N_c \to \infty$. These emissions are repeated recursively until a cut-off scale $Q_0^2$.

The total emission probability for a dipole is calculated from the sum of the two splitting functions from the two sides of the dipole.

Each emission with a non-vanishing momentum involves a recoil. Gluons carry a colour and an anticolour and are therefore, connected with two colour lines. The recoil of a dipole containing a gluon may therefore, affect the subsequent evolution of the other dipole connected to the gluon. To prevent that, the emission of the highest transvere momentum is generated at first. This transverse momentum then functions as a upper limit for the other evolution.

In Herwig 7 the basis of the dipole shower implementation is the Catani-Seymour subtraction kernel [26].

## 3.3. Hadronization

The partonic final states evolved from the parton shower have to be transformed into the final state particles as measured in the detector. This happens in the soft regime, where perturbation theory is not valid. Hence, one has to make use of phenomenological models. Different Monte Carlo event generators use different hadronization models. In Pythia [27], for instance, the Lund-String model [28] is implemented. In contrast, Herwig makes use of the so-called cluster model [29], which is based on the preconfinement property of the parton showers [30]. Such a hadronization model was first proposed in [31] and then incorporated into a lepton event generator in [32] and [33].

The preconfinement property states that for any shower at any evolution scale $Q^2$ the partons can be arranged in colour-singlet states, which have an asymptotically universal invariant mass distribution. This implies that the mass distribution depends neither on the scale $Q^2$ nor on any property of the hard process or the shower itself.

The colour structure is considered in the $N_C \to \infty$ limit, where it is a set of colour lines connecting colour-charged partons with anticolour-charged partons to colour-singlets. Since in this limit gluons always carry both anti-colour and colour, the remaining gluons are each split non-pertubatively into quark-antiquark pairs. Then the parton pairs connected by colour lines form colour-neutral clusters. These clusters subsequently decay into excited states of hadrons. These excited states again successively decay into final state particles observed in the detector. Clusters which are too heavy to perform this decay directly first fission into a pair of lighter clusters. Also colour reconnection can be applied before cluster fission and cluster decay. A simplified sketch of the hadronization process without colour reconnection is shown in figure 3.2. In the following subsections the individual steps of the hadronization process are discussed in more detail.

### 3.3.1. Gluon Splitting and Cluster Finding

In the $N_C \to \infty$ limit gluons are always part of an anticolour and a colour line and thus, the colour structure is planar. First the remaining gluons from the parton shower are split non-perturbatively into quark-antiquark pairs. The splitting is done isotropically in the restframe of each gluon. For this to be possible, the gluons acquire a constituent mass at this stage. The splitting can only produce the lighter quark flavours: up, down and strange. The flavours are produced with different weights.

After the splitting only colour-connected quark-antiquark pairs are left. The colour-connected particle pairs each are gathered into clusters with mesonic quantum numbers. These clusters are colour-singlets, i.e. colour-neutral. The momentum of a cluster is determined by the sum of the momenta of its components. Due to the preconfinement property the mass distribution of the cluster does not depend on the hard process or properties of the shower. Furthermore, it can be shown that high cluster masses are suppressed and the mass distribution peaks at the order of $\mathcal{O}(1-3\,\text{GeV})$ [34].

Clusters that are formed in this first cluster finding process are referred to as primary clusters.
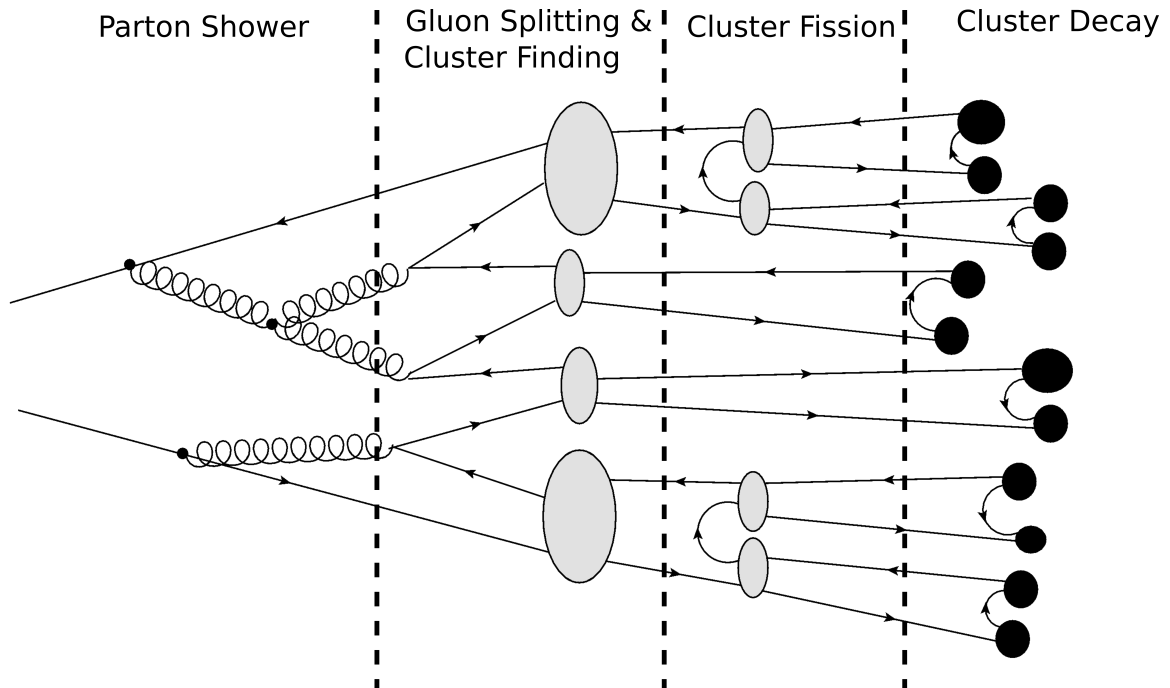
Figure 3.2.: Schematic overview of the hadronization process in Herwig. First remaining gluons are split into quark-antiquarks pairs. Then colour-connected partons form clusters, which either decay directly into a pair of excited hadrons or fisson into two lighter clusters first.

At this point, one aspect should be mentioned that has been neglected so far. Not every primary cluster necessarily contains a quark and anti-quark and has mesonic quantum numbers. There are also primary clusters containing a quark-diquark pair (an antiquark-antidiquark pair respectively) with baryonic quantum numbers. A (anti)diquark is a theoretical state of two (anti)quarks grouped together. Diquarks carry anticolour-charge and antidiquarks colour-charge. In Herwig the beam remnants are treated as diquarks and thus, there are diquarks in primary clusters, when there are beam remnants involved in the process.

### 3.3.2. Colour Reconnection

The basic idea of *colour reconnection* is to consider different colour-connection topologies than the one predefined by the parton shower. This is done by exchanging components of different primary clusters with each other to form new possible colour-neutral states. This is especially interesting, because the hard process and the underlying event otherwise exist "side by side" without influencing each other. In primary clusters there are no partons from the different parts together. Thus, colour reconnection is a way to connect the underlying event with the hard process.

There are different models for performing colour reconnection. In Herwig 7.2.2 there are three such models available, all based on reducing the invariant mass or the inner rapidity distance of the clusters respectively. Within this thesis Herwig was extended by

a further colour reconnection algorithm, which is discussed in detail in chapter 4. This sections looks at the three models that were already in place, namely the *plain model* [35], the *statistical model* [35] and the *baryonic model* [36]. Where the last one is used by default in Herwig and is so far the only one which allows the production of clusters with baryonic quantum numbers. It should be mentioned that a further model has recently been developed based on space-time [37]. However, it is not yet available in the current Herwig release, since it is still in the process of analysis, tuning and further development.

### 3.3.2.1. Plain Colour Reconnection

This algorithm aims to reduce the sum of invariant cluster mass, which is referred to as colour length $\lambda$:

$$\lambda = \sum_{i}^{N_{\mathrm{cl}}} M_i^2, \tag{3.18}$$

where $N_{\mathrm{cl}}$ is the number of clusters. This leads to a shift towards lighter clusters.
The algorithm works like follows: First the clusters are placed in a random order to avoid systematic biases.
Then the first cluster in the list, which is labeled as cluster $A$, is picked and a suitable reconnection partner is searched for it by going through all of the other clusters in the list step by step. For each possible partner the sum of the invariant masses of the two clusters is calculated: $M_A + M_B$. Then the new possible cluster configuration with the two clusters $C$ and $D$ is considered and also the sum of their invariant masses: $M_C + M_D$. If the new cluster configuration leads to a lower sum of invariant mass, i.e. $M_C + M_D \leq M_A + M_B$ and $C$ and $D$ are colour-singlets, then cluster $B$ is marked as a possible reconnection partner for $A$.
If more than one possible reconnection partner for cluster $A$ is found, the one which leads to the lowest sum $M_C + M_D$ is chosen. The reconnection is accepted with a certain probability $p_{reco}$, which is a free parameter of the model.
The whole procedure is repeated for each cluster in the list.

### 3.3.2.2. Statistical Colour Reconnection

In this model, colour reconnection is seen as a minimization problem of the colour length $\lambda$, defined in equation 3.18. Since there is a large amount of clusters in hadron collisions, a brute force approach by calculation all possible cluster configurations is not a suitable solution. Instead the statistical colour reconnection model makes use of a simulated annealing algorithm [38] to approximate the global minimum of $\lambda$.
The algorithm picks random pairs of clusters as reconnection candidates and any reconnections that would produce colour-octets are vetoed. The reconnection is always accepted, if it lowers the colour length. If it would raise the colour length it is accepted with the probability

$$p = \exp\left\{-\frac{\lambda_2 - \lambda_1}{T}\right\} \tag{3.19}$$

with $\lambda_1$ and $\lambda_2$ being the colour length before and after respectively the reconnection. $T$ is the so-called temperature, which controls the acceptance of configurations with higher $\lambda$. It is gradually reduced during the process and thus, the probability for higher-$\lambda$ configurations is also reduced. In that way the algorithm terminates with time. The possibility to accept a reconnection that would raise $\lambda$ prevents being caught in a local minimum.

### 3.3.2.3. Baryonic Colour Reconnection

A recent extension of Herwig was the baryonic colour reconnection model [36]. In contrast to the other two colour reconnection models, it allows the generation of (anti)baryonic clusters consisting of three quarks or antiquarks respectively. Further it is not based on the colour length, since due to the relative high invariant mass of baryonic clusters, this is not reasonable. Instead the rapidity $y$ with respect to the z-axis (beam axis) is considered as the key quantity. The rapidity $y$ is given by:

$$y = \frac{1}{2}\ln\left(\frac{E + p_z}{E - p_z}\right). \tag{3.20}$$

The algorithm aims to reconnect clusters in such a way that the rapidity distance between the components within a cluster is reduced. That means that the components should approximately populate the same phase space region.
Initially, analogous to the plain colour reconnection model, the clusters are placed in a random order. Then the first cluster in the list, again referred to as cluster $A$, is considered first. Cluster $A$ is boosted in its rest-frame, where the quark $q_A$ and the antiquark $\bar{q}_A$ are back-to-back. The direction of the antiquark $\bar{q}_A$ is defined as the z-axis. Then for each other cluster $B$ the rapidity of its quark $q_B$ and antiquark $\bar{q}_B$ with respect to the z-axis and in the rest-frame of cluster $A$ is calculated. There are three different possible outcomes:

1.) $y(q_B) > 0$ and $y(\bar{q}_B) < 0$, which means that $q_B$ is in rapidity direction of $\bar{q}_A$ and $\bar{q}_B$ is in rapidity direction of $q_A$. Cluster $B$ is considered for **mesonic** reconnection with cluster $A$ and referred to as mesonic candidate.

2.) $y(q_B) < 0$ and $y(\bar{q}_B) > 0$, which means that $q_B$ is in rapidity direction of $q_A$ and $\bar{q}_B$ is in rapidity direction of $\bar{q}_A$. Cluster $B$ is considered for **baryonic** reconnection with cluster $A$ and referred to as baryonic candidate.

3.) Neither 1.) nor 2.) is fulfilled. Cluster $B$ is not considered for any reconnection with cluster $A$.

In order to decide which clusters are finally chosen for reconnection, the total rapidity sum $y_{tot} = |y(q_B)| + |y(\bar{q}_B)|$ is considered, where again cluster configurations containing colour-octet states are vetoed. If the two clusters with the highest sum $y_{tot}$ are baryonic candidates, baryonic reconnection takes place with probability $p_B$. If the cluster with the highest sum $y_{\text{tot}}$ is a mesonic candidate, mesonic reconnection takes place with probability $p_M$. Again, analogous to the plain colour reconnection model, the procedure is repeated for each cluster in the list.

However, baryonic and antibaryonic clusters produced during the algorithm are excluded from further reconnections. Thus, this model contains transitions from mesonic to baryonic clusters but no retransitions from baryonic to mesonic clusters. Hence, it must be noted that this model may lead to a systematic bias towards baryonic clusters. However, the baryonic colour reconnection model achieved significant improvement in the description of various observables.

### 3.3.3. Cluster Fission

There is small fraction of clusters which has to fission into lighter - less excited - clusters, since they carry too much mass to decay directly into hadrons. Thus, cluster fission is a transition from particles with high energy to a greater number of particles with lower energy. Since the formation of hadrons is carried out non-perturbatively, it is reasonable to avoid high energy scales. To decide whether or not a cluster fissions the following condition is used:

$$M^{Cl_{\text{pow}}} \geq Cl_{\max}^{Cl_{\text{pow}}} + (m_1 + m_2)^{Cl_{\text{pow}}}, \tag{3.21}$$

where $M$ is the invariant mass of the considered cluster and $m_1$ and $m_2$ are the invariant masses of the cluster components. $Cl_{\text{pow}}$ and $Cl_{\max}$ are free parameters which are different for different flavours. If condition 3.21 is fulfilled for a cluster, the following fission process is applied on it: First of all, a quark-antiquark pair or a diquark-antidiquark pair is generated from the vacuum, where only light flavours are allowed (up, down and strange). The probability for generating a certain flavour is also controlled by a parameter of the model. Then two new clusters are formed, each containing a component of the parent cluster and the matching partner of the quark-antiquark-pair. The mother cluster is subsequently replaced by the two children in the event record. Due to diquark production, clusters with baryonic quantum numbers may be produced.

The masses of the new clusters are chosen according to:

$$M_1 = m1 + R_1^{\frac{1}{P_{\text{split}}}} \cdot (M - m_1 - m_q), \tag{3.22}$$

$$M_2 = m2 + R_2^{\frac{1}{P_{\text{split}}}} \cdot (M - m_1 - m_{\bar{q}}), \tag{3.23}$$

where $M_1$ and $M_2$ denote the masses of the new clusters and $m_q$ and $m_{\bar{q}}$ denote the masses of the generated parton pair. $R_1$ and $R_2$ are uniformly distributed random numbers in the interval [0,1]. $P_{\text{split}}$ is the so-called splitting parameter which controls the distribution of cluster masses and is also flavour-dependent.

There are additional constraints for the masses of the child clusters. The sum of the two new cluster masses has to be less than or equal to the mass of the parent cluster, i.e. $M \geq M_1 + M_2$, and the mass of each cluster is required to be greater than the sum of the masses of its components.

### 3.3.4. Cluster and Hadron Decay

Once the cluster fission is complete, the clusters decay into excited hadrons. Usually one cluster decays in a pair of excited hadrons. This is to ensure momentum and energy conversation. The types of hadron depends on flavour and spin of the partons in the clusters and also on the available phase space.

First, baryonic clusters produced during colour reconnection, which contain three quarks are transformed to clusters containing a quark and diquark. For the actual decay, similar to cluster fission, a quark-antiquark pair or a diquark-antidiquark pair is produced from the vacuum, where again only the light flavours up, down, and strange are allowed with different weights. A sketch of all possible decay combinations is shown in figure 3.3. It can be seen that the emerging hadron pair is either a pair of (anti)mesons, an antibaryon-baryon pair, a (anti)meson-baryon pair or a (anti)meson-antibaryon pair. However, antibaryon-antibaryon and baryon-baryon pairs do not occur. At this point, it is anticipated that this pairwise decay into hadrons might entail unwanted correlations. Especially, when the colour reconnection model is also considered. Because of the colour reconnection process, partons which are close in rapidity tend to be together in clusters. And subsequently, these close partons hadronize together. Thus, strong correlations for near-side particles might arise.

The clusters decay isotropically in their rest-frame. Hadrons from clusters containing a parton produced in the perturbative stage retain the direction of this parton, but with a small Gaussian smearing, whereby the smearing angle is randomly chosen depending on the flavour of the parton.

Clusters which are too light to decay directly into two hadrons decay instead into the lightest allowed hadron. In order to give them the correct invariant mass, their energy and momentum is reshuffled with clusters neighbouring them.
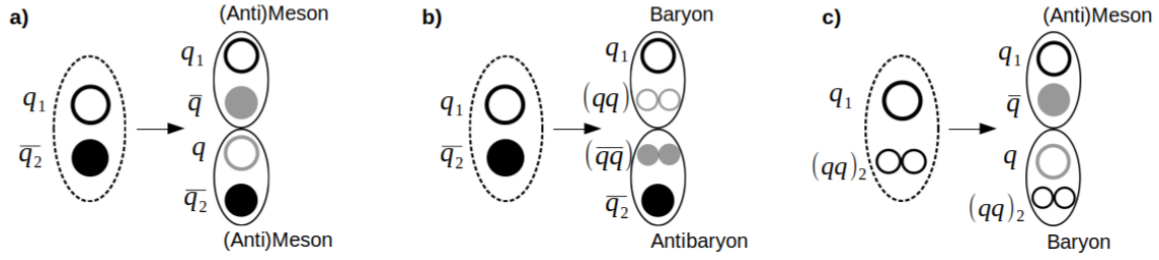
Figure 3.3.: Possible pairwise cluster decays. Depending on the cluster components and the produced quark-antiquark pair or diquark-antidiquark pair respectively, either a) two (anti)mesons, b) a baryon-antibaryon pair or c) a (anti)meson-baryon pair or a (anti)meson-antibayron pair (in case of a cluster with antibaryonic quantum numbers) respectively is produced. Baryon-baryon and antibaryon-antibaryon pairs do not occur.

These hadrons originating from the cluster decays are excited hadrons and hence unstable. As a result, they decay again into the final-state particles measured in the detector. Both strong and electroweak decays happen and thus, not only hadrons but also, for instance, leptons are produced. The model for hadron decays used in Herwig is described in [1]. Additionally, a description for $\tau$-decays can be found in [39].

## 3.4. Underlying Event

In hadron colliders an event will involve not only the hard process, but also the so-called *underlying event*. In collider experiments the underlying event is defined as the sum of incidents which are not related to the hard process of interest. The colliding hadrons are composite particles and thus, all constituents may interact with each other. Therefore, additional hard processes in the perturbative regime might happen but also soft interactions at lower energies. For high center-of-mass energies, the probability that more hadronic interactions happen than only the hard event is significant. These additional interactions are the dominant part contributing to the underlying event. Therefore, it is crucial for an accurate simulation to ensure that there is a good description of these interactions.
The underlying event is modeled with *multiple parton interactions* (MPIs). The MPI-model used in Herwig is based on the *eikonal model* [40–42]. It consists of two separate parts, a perturbative and a non-perturbative one. Here the transverse momentum of the respective interaction is decisive. If it is above a certain threshold momentum $p_T^{\min}$, the interaction is modelled as a QCD $2 \rightarrow 2$ interaction. These perturbative interactions are referred to as *semi-hard* interactions. However, if the transverse momentum is below $p_T^{\min}$, the interaction is referred to as *soft interaction*. Before the release of Herwig 7.1 the default model for these soft interactions were elastic gluon scatterings [43]. This model can still be chosen by the user in the current version of Herwig. However, with the mentioned release a new model was introduced [44]. While in the old model for every soft interaction a pair of gluons is produced, in the new model a pair of quarks and a number of gluons, whose transverse momentum is restricted by the threshold momentum $p_T^{min}$, is produced.

The gluons are ordered in rapidity in such a way that the rapidity distribution of the subsequently produced particles is roughly flat.

The threshold momentum is not the same for each simulated collision but depends on its center-of-mass energy $\sqrt{s}$ and is extrapolated by a power law:

$$p_T^{\min} = p_{T,0}^{\min} \cdot \left( \frac{\sqrt{s} + b}{E_0} \right)^c, \tag{3.24}$$

where $p_{T,0}^{\min}$ is the value of $p_T^{\min}$ around the reference scale $E_0$. $b$ is an offset, which is necessary for fitting $p_T^{min}$ for small center-of-mass energies $\sqrt{s}$. $p_{T,0}^{\min}$, $E_0$, $b$ and the power $c$ are correlated parameters of the model. Besides these, the inverse hadron radius $\mu^2$ is also an important parameter for the MPI model, since it controls the matter distribution in the proton. The parameters of the MPI and also of the colour reconnection have been tuned to minimum bias and underlying event data [45] to ensure a good description of data. It is worth mentioning that it can be observed that $\mu^2$ and $p_{T,0}^{min}$ are correlated for some observables.

## 3.5. Minimum Bias Events and Diffractive Model

In experiments *minimum bias* defines a class of events done with a trigger which has as little bias as possible. Hence, there is no certain hard process in focus. Instead, the aim is to be as inclusive as possible. Such minimum bias events where no hard process occurs make up the bulk of events at high-energy experiments.

In Herwig minimum bias events are simulated with the MPI model. Since the software architecture of Herwig requires a "hard process" to split up the colliding hadrons and initiate the MPIs, a dummy matrix element is used to replace the actual hard process. Resulting in a situation where partons with no transverse momentum are taken from the hadrons.

However, this is not sufficient to describe all minimum bias observables accurately. Especially for events with a large pseudorapidity gap an alternative approach is necessary. Diffraction describes hadron collisions where no perturbative electroweak or strong interaction among the partons occurs but where one or both of the hadrons are broken up.

In *Regge theory* diffraction is modeled by an exchange of pomerons which are hypothetical colour-neutral strong-interacting particles. There are three different types of diffraction: (i) single diffraction, where only one hadron dissociates, i.e. $A + B \rightarrow A + X$ (ii) double diffraction, where both hadrons dissociate , i.e. $A + B \rightarrow X + Y$ and (iii) central diffraction, where an active region in-between the two hadrons appears, i.e. $A + B \rightarrow A + X + B$.

So far in Herwig only single diffractive and double diffractive events are available. The dissociation of a proton is simulated by a decay into a quark-diquark pair moving collinar to the mother proton. This pair is then transformed into a cluster and thus, in the subsequent hadronization process decays into one, two or more hadrons. Detailed descriptions of the diffractive model of Herwig can be found in [46] , where it was first introduced, and in [47]. To vary the ratio between diffractive and non-diffractive events in Herwig there is a model parameter called `DiffractionRatio`, which represents the ratio of the diffractive

and the non-diffractive cross section. Approximately 20 - 25 % of the events are diffractive.

In order to simulate an event as exclusive as possible, and to describe a hard process and its underlying event in all detail, it is crucial that not only the high-energy parts of an event are simulated accurately but also the soft parts. For the second, minimum bias observables are rigorous arenas to test any new phenomenological model.

# 4. Baryonic-Mesonic Colour Reconnection Model

Since colour reconnection models entail that different parts of the event interfere and hadronize together, they are indispensable for describing data from hadron colliders. A prominent example is the distribution of mean transverse momentum over the number of charged particles $< p_T > (N_{\text{ch}})$. For independent interactions $< p_T >$ would not depend on $N_{\text{ch}}$. Due to a large spacetime overlap of the individual interaction this is not true for reality. And thus, colour reconnection is essential for this observable. In the colour reconnection process the multiplicity is reduced due to smaller clusters and the available transverse momentum is shared between less particles. Thus, $< p_T >$ rises for the same $N_{\text{ch}}$.

An overview of colour reconnection in Herwig and the implemented models is given in section 3.4. In the following, clusters consisting of a quark and an antiquark are referred to as mesonic clusters, while clusters consisting of three quarks or three antiquarks respectively are called baryonic or antibaryonic respectively.

Adding the baryonic colour reconnection model (see subsection 3.3.2.3) to Herwig led to a significant improvement of the description of various observables. As an example in figure 4.1 the charged multiplicity for $N_{ch} \geq 1$ using the plain and the baryonic colour reconnection respectively is plotted and compared to data from ATLAS [48]. The curve produced with baryonic colour reconnection fits the data better. However, while with plain colour reconnection the high charge multiplicities are overestimated, with the baryonic colour reconenction they are underestimated. Thus, there is still room for improvement. Since baryonic clusters produced during the algorithm are excluded from further reconnections, the model may lead to a systematic bias towards baryonic clusters. It is reasonable to assume that a model implying re-reconnection to mesonic clusters may compensate for overcompensation as observed in figure 4.1.

In the following we implement such a model into Herwig, the so-called *baryonic-mesonic colour reconnection model.* It incorporates baryonic clusters in the reconnection process. Besides re-reconnection from baryonic to mesonic clusters, reconnection from baryonic clusters to differently arranged baryonic clusters and also between mesonic and baryonic clusters are allowed. A similar idea was already pursued in [49], where baryonic reconnection from mesonic to baryonic clusters as well as re-reconnection from baryonic to mesonic clusters were incorporated in a simulated annealing algorithm [38]. However, here we use a slightly different approach.

In the following, we first present the fundamentals and subsequently the algorithm. We tune the model parameters to data and discuss the results, whereby we also consider analyses not used for the tuning procedure.
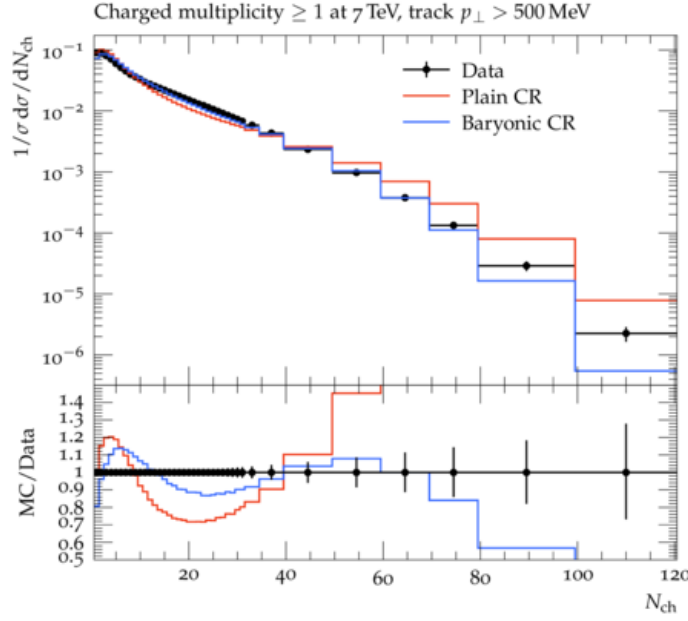
Figure 4.1.: Comparison of Herwig 7.2 with plain and baryonic colour reconnection for charged multiplictiy distribution for $N_{ch} \geq 1$ and $p_T > 500$ measured by ATLAS. The baryonic colour reconnection model lead to a better description of data. The plot was done using RIVET [50].

## 4.1. Fundamentals

The plain and the statistical colour reconnection model aim to reduce the invariant cluster mass. Since baryonic clusters carry a relatively high mass, for the baryonic colour reconnection model the rapidity distance was introduced as a reconnection criterion. For the baryonic-mesonic model we use a related but slightly different criterion: the displacement $\Delta R$ which reads for two partons $i$ and $j$

$$\Delta R_{ij}^2 = \Delta Y_{ij}^2 + \Delta \phi_{ij}^2. \tag{4.1}$$

Here $\Delta Y_{ij}$ is the rapidity distance between the considered quarks $(y_i - y_j)$ relative to the beam axis, where the rapidity reads

$$y = \frac{1}{2} \ln \left( \frac{E + p_z}{E - p_z} \right). \tag{4.2}$$

$E$ is the energy of the considered parton and $p_z$ is the momentum with respect to the z-axis, i.e. beam-axis. The rapidity is a measure for the relativistic velocity of a particle. For a particle with small momentum with respect to the z-axis it approaches zero. In contrast, if the particle moves along the beam-axis the rapidity goes towards infinity. Thus, the rapidity indicates the direction of a particle along the beam-axis.

In the second term of equation 4.1 $\Delta \phi_{ij}$ refers to the azimuthal angular distance of the two partons $\phi_i - \phi_j$. The azimuthal angle is the angle "around" the beam-axis. Hence, the

rapidity - as a measure for the direction along the beam-axis - in combination with the azimuthal angle provides an accurate description of the direction in which a particle is moving. Figure 4.2 is intended to illustrate that. A colour reconnection model based on the displacement $\Delta R$ considers clusters for reconnection, if the involved partons go to the same direction.
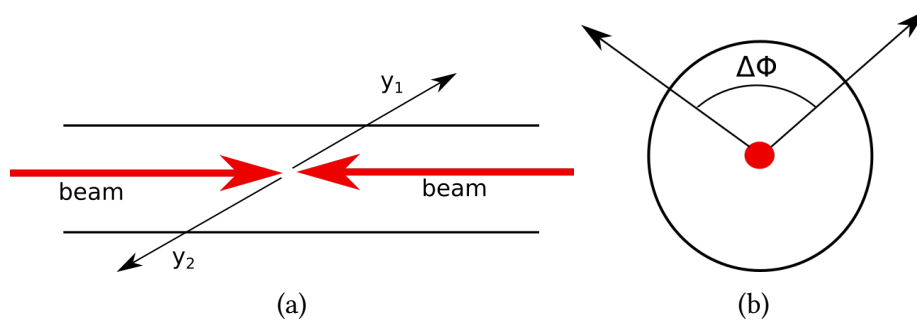


Figure 4.2.: Illustration of rapidity (a) and azimuthal angle (b). The rapidity is a measure for the direction of a particle along the beam-axis. The azimuthal angle gives the direction around the beam-axis.

## 4.2. Algorithm

The colour reconnection process and thus the baryonic-mesonic colour reconnection model starts immediately after the cluster finding (see subsection 3.3.1) in the hadronization process. Once the perturbative evolution of the parton shower has terminated and the gluons are split into quark-antiquark pairs, all colour-connected partons form colour-neutral clusters. Technically, the resulting primary clusters are combined in a so-called cluster-vector and this is passed on to the colour reconnection model, which is allowed to change the predefined cluster configuration.

First a brief overview of the basic steps of the baryonic-mesonic colour reconnection algorithm is given. The individual steps are explained in more detail below. The algorithm goes through the following steps:

1.) Pick a random combination of clusters, which should be either *three mesonic* clusters, *two (anti)baryonic* or *one mesonic cluster mesonic and one (anti)baryonic cluster*.

2.) Determine the displacement $\Delta R$ for each picked cluster and calculate the sum.

3.) Go through all other possible cluster configurations for the constituents chosen by step 1.), each time calculating the sum for $\Delta R$. Configurations which would result in colour-charged clusters are automatically vetoed.

4.) If a possible reconnection leads to a lower total $\Delta R$-sum than the original configuration, it is considered for reconnection. In the case of multiple such configurations, the one with the lowest total $\Delta R$ is chosen.

5.) The reconnection is accepted with a certain probability depending on the kind of reconnection.

We decide not to include the case of only two mesonic clusters considered for mesonic reconnection directly. This is to keep the algorithm as simple as possible. Three mesonic clusters are needed to reconnect to a baryonic and an antibaryonic cluster. Thus, in the case of three mesonic clusters, we are able to consider baryonic and mesonic reconnection simultaneously. Also, the case of two clusters perform mesonic reconnection is already included indirectly when one cluster remains unchanged in the case of mesonic reconnection.
Additionally, clusters containing diquarks are generally excluded from reconnection. This is the case in all implemented models and is conventionally justified as follows: diquarks at this stage of simulation always originate from the hadron remnants and thus are relatively far away from other clusters.

The steps in the baryonic-mesonic reconnection algorithm are repeated several times. The exact number of iterations $N_{\text{steps}}$ is determined by

$$N_{\text{steps}} = f_{\text{step}} \cdot N_{\text{cl}}^2, \tag{4.3}$$

where $N_{\text{cl}}$ is the total number of clusters in the event and $f_{\text{step}}$ is the so-called `StepFactor`, which is a free parameter of the model.

### 4.2.1. Picking random Clusters

Since the algorithm only considers specific configurations of the randomly picked clusters previously mentioned, it is not sufficient to simply pick two or three clusters from the list. Either three mesonic, two (anti)baryonic or a mesonic and a (anti)baryonic cluster are needed and thus, the algorithm is illustrated in a simplified way in figure 4.3.
Initially the clusters are shuffled so that they are in a random order. The first cluster not containing a diquark is added to the list of picked clusters in any case, likewise the second one. If one of them or both are (anti)baryonic, the picking procedure terminates. Now, we have either two (anti)baryonic clusters or a (anti)baryonic and a mesonic cluster considered for reconnection. If the first two clusters are mesonic, we go through the rest of the clusters until a third mesonic one is found. In that case, three mesonic clusters are considered for reconnection.
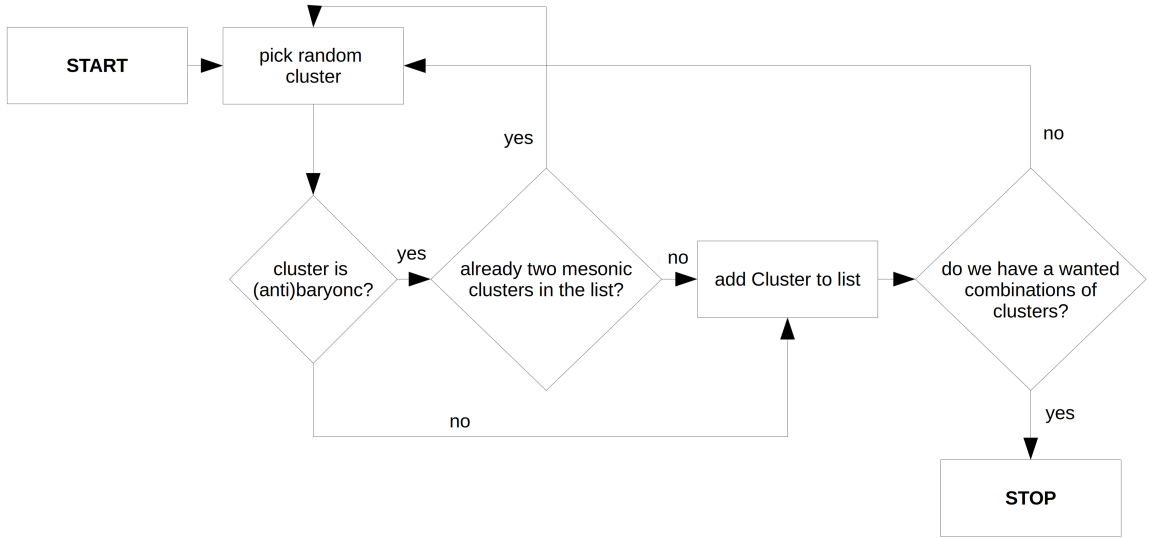
Figure 4.3.: Schematic overview of the algorithm picking the cluster combination considered for reconnection. The algorithm terminates, when either three mesonic, two baryonic, or a mesonic and a baryonic cluster are in the list.

## 4.2.2. Determining the Displacement

As mentioned above, the equation 4.1 is used as a measure of the displacement within a cluster. For mesonic clusters this is trivial, since only $\Delta R$ between the quark and the antiquark has to be calculated. (Anti)baryonic clusters on the other hand have three components ($q_1$, $q_2$, $q_3$). Therefore, the total displacement $\Delta R_{\text{tot}}$ is given by the sum of all displacements between the individual quarks and thus, reads

$$\Delta R_{\text{tot}} = \Delta R_{1,2} + \Delta R_{1,3} + \Delta R_{2,3}. \tag{4.4}$$

In order to make (anti)baryonic and mesonic cluster-configurations comparable, a factor $\omega_{\text{BM}}$ regulating the weight of displacements of the (anti)baryonic clusters with respect to the mesonic ones has to be introduced. To illustrate that, the possible configurations of three quarks (1, 2, 3) and three antiquarks ($\bar{1}$, $\bar{2}$, $\bar{3}$ ) are considered. A possible configuration with three mesonic clusters is, for instance, $1\bar{1}$, $2\bar{2}$, $3\bar{3}$. Here it is assumed that the three considered quark-antiquark pairs form colour singlets. In this case the total displacement $\Delta R_{\text{tot}}^{\text{mes}}$ is determined by the sum of the displacements of the individual clusters,

$$\Delta R_{\text{tot}}^{\text{mes}} = \Delta R_{1,\bar{1}} + \Delta R_{2,\bar{2}} + \Delta R_{3,\bar{3}}. \tag{4.5}$$

For the same six partons, only one baryonic cluster configuration is possible consisting of a baryonic cluster (123) and an antibaryonic cluster ($\bar{1}\bar{2}\bar{3}$). The total displacement $\Delta R_{\text{tot}}^{\text{bary}}$ is again determined by the the sum of the displacements of the baryonic and the antibaryonic cluster $\Delta R_{1,2,3}$, $\Delta R_{\bar{1},\bar{2},\bar{3}}$ respectively and due to equation 4.4 reads

$$\Delta R_{\text{tot}}^{\text{bary}} = \Delta R_{1,2,3} + \Delta R_{\bar{1},\bar{2},\bar{3}} = \Delta R_{1,2} + \Delta R_{1,3} + \Delta R_{2,3} + \Delta R_{\bar{1},\bar{2}} + \Delta R_{\bar{1},\bar{3}} + \Delta R_{\bar{2},\bar{3}}. \tag{4.6}$$

If equations 4.5 and 4.6 are now considered, it immediately becomes apparent that $\Delta R_{\text{tot}}^{\text{mes}}$ is the sum of three individual displacements, while $\Delta R_{\text{tot}}^{\text{bary}}$ is the sum of six displacements. Therefore, it seems natural to set the weight $\omega_{\text{BM}}$ to 1/2, i.e. whenever the displacement of (anti)baryonic and mesonic clusters are compared, the displacement-values of the (anti)baryonic clusters are multiplied by 1/2. Based on this simple consideration $\omega_{\text{BM}}$ was specified to be 1/2 during the implementation of the baryonic-mesonic colour reconnection model. However, this does not necessarily have to be the best choice. It is possible that a different value entails a better description of the meson-baryon ratio in hadron-collisions. The choice of this parameter could play a role in future tunes and improvements of the model. We leave this avenue open to further investigations in the future.

### 4.2.3. Reconnection Configurations

We give a short overview over the possible reconnection configurations occurring in the model. They are summarized in table 4.1, where M refers to a mesonic cluster, B to a baryonic and aB to an antibaryonic cluster.
There are four different configurations for the randomly picked clusters considered for reconnection.

1.) In the case of three mesonic clusters, the clusters might reconnect to three different mesonic clusters or to an antibaryonic and a baryonic cluster. For the six quarks considered here, there are six mesonic cluster configurations, one of which is the inital one, and one baryonic. If the best reconnection option is mesonic, the reconnection is accepted with probability $p_{M,M}$, and if it is baryonic with probability $p_{M,B}$.

2.) If we consider a mesonic and a (anti)baryonic cluster, they might reconnect to a different mesonic and anti(baryonic) cluster. In that case, there are three reconnection configurations that have to be considered, where the (anti)quark of the mesonic cluster is exchanged with each parton of the (anti)baryon. A possible found reconnection option is accepted with probability $p_{MB,MB}$.

3.) If the considered clusters are a baryonic and an antibaryonic cluster, they might reconnect to three mesonic clusters. In that case, there are six possible configurations as to how the quarks from the baryonic cluster form mesonic clusters with the antiquarks from the antibaryonic cluster. Here the reconnection is accepted with probability $p_{B,M}$.

4.) Finally, two baryonic or antibaryonic clusters respectively can be considered for reconnection. They have nine reconnection configurations to form two different baryonic or antibaryonic clusters respectively. If a possible reconnection is found, it is accepted with probability $p_{B,B}$.

The reconnection probabilities are free parameters of the model. Additionally, there is the `StepFactor` (see equation 4.3), which controls the number of iterations. Thus, there are six parameters in the model that must be carefully chosen to get a good description of data.

Table 4.1.: Overview of the possible reconnection configurations. M refers to a mesonic cluster, B to a baryonic and aB to an antibaryonic cluster. The third column gives the corresponding reconnection probability parameter.

| Before reconnection | After reconnection | Reconnection probability |
|---|---|---|
| 3 M | 3 M' | $p_{M,M}$ |
| 3 M | 1 B + 1 aB | $p_{M,B}$ |
| 1 M + 1 (a)B | 1 M' + 1 (a)B' | $p_{MB,MB}$ |
| 1 B + 1 aB | 3 M | $p_{B,M}$ |
| 2 (a)B | 2 (a)B' | $p_{B,B}$ |

## 4.3. Tuning and Results

The values of the new model parameters have to be constrained. Due to the high numbers of parameters, we tune the parameters to experimental data using the current version of the PROFESSOR tuning system [51] in combination with AutoTunes framework [52]. The used analyses are provided by Rivet [50]. The tuning is performed for $\sqrt{s}$ = 7 TeV center-of-mass energy and with minimum bias data. First we briefly describe the tuning procedure, subsequently we present the tuning results and finally we discuss the output for analyses not included in the tuning procedure.

### 4.3.1. Tuning Procedure

Since we expect the model to have significant impact on the multiple parton interactions, key parameters of the MPI-model are included in the tuning procedure, namely the inverse proton radius $\mu^2$ and $p_{T,0}^{\min}$. This results in a total of 8 parameters:

- the five probabilities of the baryonic-mesonic colour reconnection model: $p_{M,M}$, $p_{M,B}$, $p_{MB,MB}$, $p_{B,M}$ and $p_{B,B}$

- the StepFactor $f_{\text{step}}$ of the baryonic-mesonic colour reconnection model, controlling the number of reconnection-iterations

- $p_{T,0}^{\min}$, parameter of the parametrisation of soft-hard-threshold transverse momentum in the MPI-model (see equation 3.24)

- the squared inverse proton radius $\mu^2$ which controls the matter distribution within the proton

As previously indicated, the factor $\omega_{\text{BM}}$ regulating the weight of displacements of baryonic clusters with respect to mesonic ones is in principle a tuneable parameter. However, in the scope of this work we fixed it to 1/2 based on considerations we made (see subsection

4.2.2). We tune to minimum bias data measured by ATLAS [53] using the results from the analyses published in [48]. In detail we use the following observables, where the weights are adjusted by AutoTunes.

- The charged pseudorapidity distributions for $N_{ch} \geq 1$, $N_{ch} \geq 2$, $N_{ch} \geq 6$ and $N_{ch} \geq 20$

- The charged transverse momentum distributions for $N_{ch} \geq 1$, $N_{ch} \geq 2$, $N_{ch} \geq 6$ and $N_{ch} \geq 20$

- The charged multiplicities for $N_{ch} \geq 1$, $N_{ch} \geq 2$, $N_{ch} \geq 6$ and $N_{ch} \geq 20$

- The average charged transverse momentum vs. number of charged particles for $N_{ch} \geq 1$ and $N_{ch} \geq 2$

AutoTunes divides the parameters to be tuned in two subsets, which are chosen in such way that strongly correlated parameters are tuned together. For each subset, a set of 500 Herwig runs with randomly distributed parameter-values is generated and then several times a subset of these runs is used to interpolate the generator response. This is done by using PROFESSOR. For each of these run combinations, again PROFESSOR is used to determine the parameter-values which lead to the smallest $X^2/N_{\mathrm{dof}}$-value, where $N_{\mathrm{dof}}$ refers to the degrees of freedom. The parameter ranges arising from the results of the individual run-subsets are then used for the next tune iteration. In total we perform two iterations. As the final result, we obtain the parameter values resulting in the smallest $X^2/N_{\mathrm{dof}}$-value as well as the whole range for the parameter values received by the set of tunes of the last iteration.

## 4.3.2. Tuning Results

The results are listed in table 4.2, where we show the parameter choice which results in the lowest $X^2/N_{\mathrm{dof}}$ value, and also the total range obtained by the total number of tunes. A small range means that the data are highly sensitive to the parameters. The default value in the current Herwig version for each parameter as well as the parameter-ranges used for tuning are also listed.

We notice that the value for the MPI-parameters do not exhibit much deviation from their default values. The tuned value for $f_{\mathrm{step}}$ is almost 1. According to equation 4.3 that means, the number of reconnection-tries is approximately the squared number of clusters in the event. This corresponds to the plain and baryonic colour reconnection model, where for each cluster the reconnection with every other cluster is checked.

Additionally, the probability-parameter for two baryonic clusters reconnecting to three mesonic clusters $p_{B,M}$ is very low. Hence, we conclude that the assumed bias towards baryonic clusters in the baryonic reconnection model is probably not a major problem. However, a different choice of the weight $\omega_{\mathrm{BM}}$ may entail diverging results. For larger $\omega_{\mathrm{BM}}$, the mesonic reconnection is preferred over the baryonic in the case of three mesonic clusters. And baryonic reconnection is only considered, when it leads to a massive decrease of displacement. Thus, increasing the value of $\omega_{\mathrm{BM}}$ could lead to a higher tuning result for $p_{M,B}$ and also to a lower value for $p_{M,M}$.

Table 4.2.: Parameter values for the baryonic-mesonic colour reconnection model tuned to minimum bias data from ATLAS [48]. The first two columns give the default values in the current Herwig version and the parameter-ranges used for tuning. Then the parameter-values resulted in smallest $X^2/N_{\mathrm{dof}}$ as well as the parameter-ranges obtained by the total number of tunes are listed.

| parameter | default value | range used for tuning | best value | range obtained by tuning |
|---|---|---|---|---|
| $p_{T,0}^{\min}$ | 2.87 | $1.0 - 5.0$ | 2.89 | $2.85 - 2.92$ |
| $\mu^2$ | 1.1 | $0.0 - 2.0$ | 1.10 | $1.08 - 1.11$ |
| $p_{M,M}$ | 0.95 [1] | $0.0 - 1.0$ | 0.56 | $0.52 - 0.57$ |
| $p_{M,B}$ | 0.7 | $0.0 - 1.0$ | 0.41 | $0.40 - 0.44$ |
| $p_{MB,MB}$ | None | $0.0 - 1.0$ | 0.09 | $0.08 - 0.11$ |
| $p_{B,B}$ | None | $0.0 - 1.0$ | 0.22 | $0.11 - 0.24$ |
| $p_{B,M}$ | None | $0.0 - 1.0$ | 0.02 | $0.00 - 0.02$ |
| $f_{\mathrm{step}}$ | None | $0.1 - 5.0$ | 1.04 | $1.03 - 1.06$ |

[1] To be exact, $p_{M,M}$ does not have a default value so far, since it is defined as the probability $3M \rightarrow 3M'$. What is given here is the default value for $2M \rightarrow 2M'$.

We obtain a satisfactory description for all considered observables. For a number of them, an improvement is achieved compared to the default of the current Herwig version, especially for the charged transverse momentum distributions. We assume that this is due to baryonic-to-baryonic reconnection, for which the value of the probability-parameter is significant higher than for the other newly introduced reconnection types. The option of baryonic-to-baryonic reconnection provides greater flexibility in the composition of baryonic clusters.

In figure 4.4 we compare the tuned new baryonic-mesonic model with the Herwig default for a selection of the considered observables. In subfigure 4.4c the charged multiplicity-distribution from figure 4.1 is shown. We observe no significant change in the distribution of this observable. In the appendix section A.1 more plots for this analysis are shown.

Below we apply the new colour reconnection model to other observables not included in the tuning procedure.
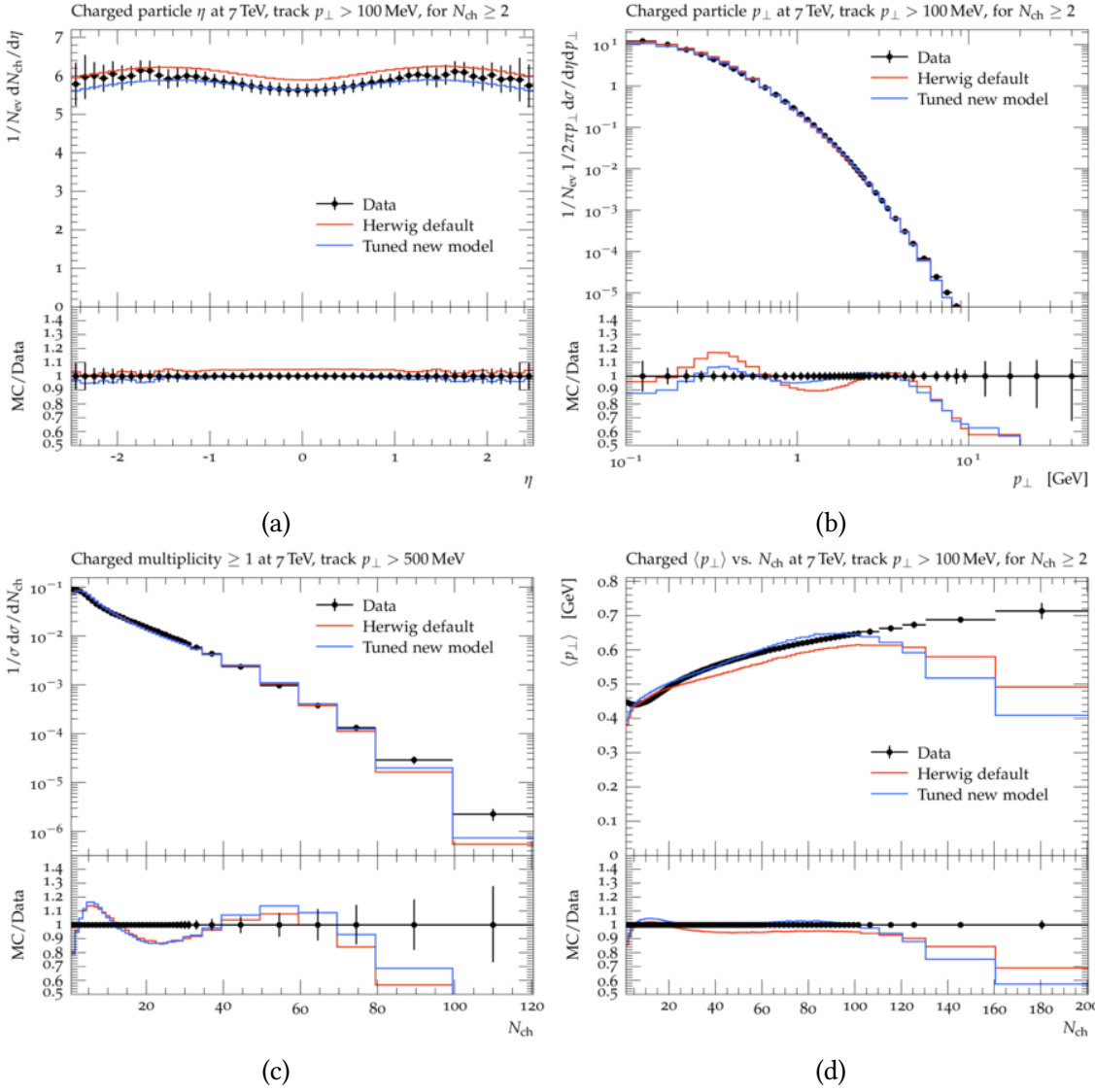
Figure 4.4.: Comparison of the default output of Herwig and the best tune for the new baryonic-mesonic colour reconnection model for minimum bias data from ATLAS.

### 4.3.3. Results for identified Particle Yields

Besides the observables we used for tuning, the yields for identified particles are key-observables for testing simulation of minimum bias events. Above we only considered observables corresponding to the totality of charged particles. Here we use data measured by ALICE and published in [54] to study the description of individual particle types. In figure 4.5 we compare the description of mid-rapidity, i.e $|y| < 0.5$, transverse momentum spectra of pions ($\pi^+ + \pi^-$), kaons ($K^+ + K^-$) and antiprotons and protons ($p + \bar{p}$) normalized to the number of inelastic collisions $N_{\mathrm{INEL}}$ for the default of the current Herwig version and the new model with the tuned parameter choice.
For $\pi^+ + \pi^-$ and $K^+ + K^-$ the description for low-$p_T$ improves slightly for the tuned new model, while we observe a deterioration for higher $p_T$. For $p + \bar{p}$ both models only roughly fit the data. In summary, although no substantial improvement can be noted, the data are still described satisfactorily and we do not see any significant deterioration. Thus, for these analyses the new model is validated.

The tuning results were also validated by cross-checks with charged-multiplicity and pseudo-rapidity distributions from ALICE [55] as well as with rapidity-gap data from ATLAS [56]. The corresponding plots can be found in the appendix sections A.2 and A.3.

## 4.4. Conclusion

We implemented a new colour reconnection model to Herwig which allows to include baryonic clusters in the reconnection process. We tuned parameters of the model to minimum bias observables and obtained a good description of this considered observables. We cross-checked the tuned model with observables of other analyses.
However, there are still many points that should be investigated with respect to the new model. So far, only its behaviour for $\sqrt{s} = 7$ TeV center-of-mass energy has been studied. In addition, further tunes may lead to an even better description. On one hand, it is interesting to perform broader tunes with more observables under consideration, e.g. observables related to the underlying event. On the other hand, promising results could be achieved by narrower tunes where only observables very sensitive to the parameters are considered.
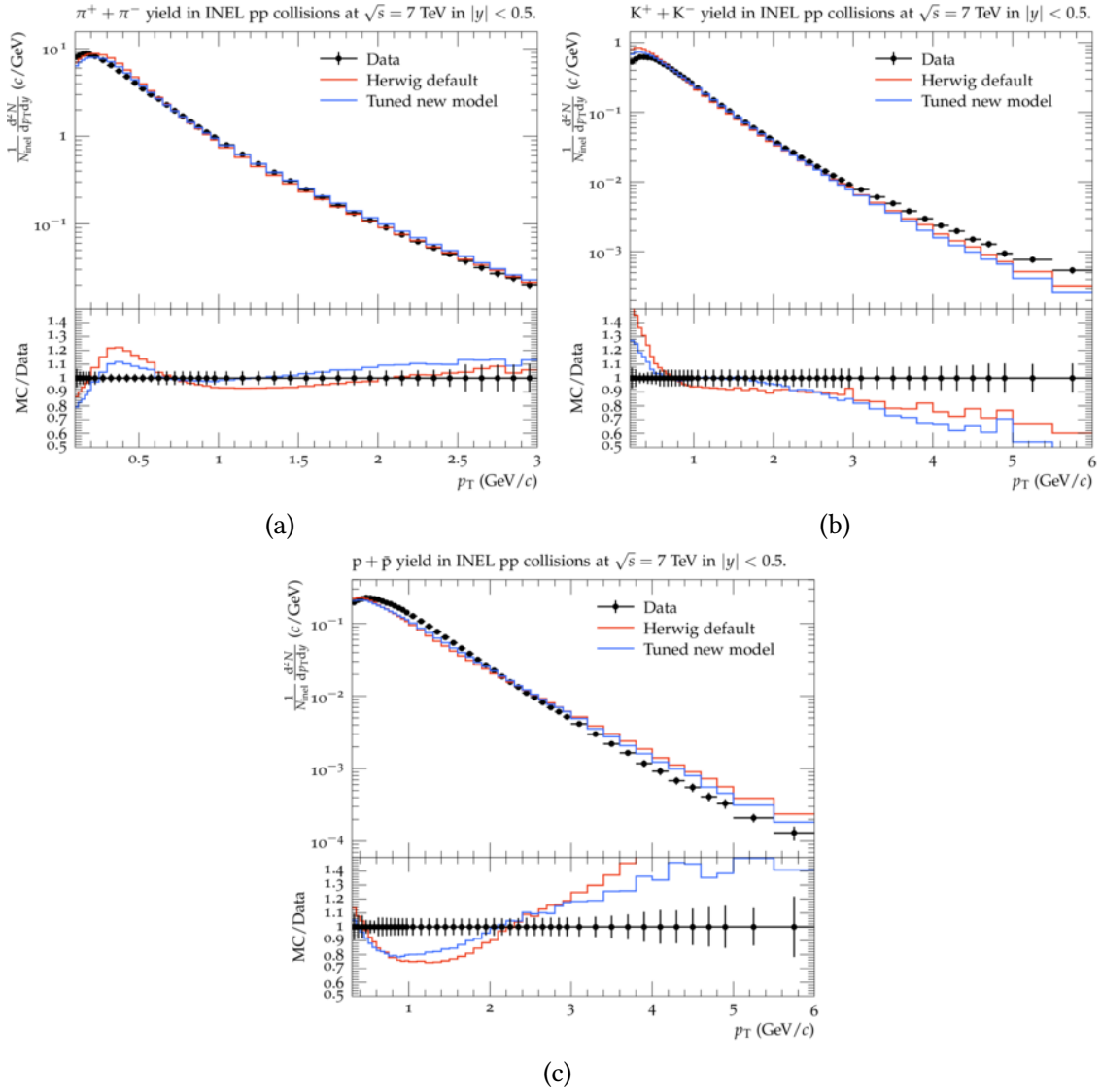
(a)

(b)



(c)

Figure 4.5.: Comparison of the default output of Herwig and the best tune for the new baryonic-mesonic colour reconnection model for transverse momentum spectra of identified particles.

# 5. Post-Hadronization Momentum Swapping

As mentioned before, minimum bias observables are rigorous arenas to test the soft physics models in the simulation process. Particle generation in hadron colliders is complex and thus, there are various minimum bias observables which have to be taken into account. There is the charged multiplicity, the particle-distribution in rapidity and the particle-distribution in transverse momentum to name just a few. In the framework of this thesis, *two-particle angular-correlations of identified particles* were considered in greater detail. In order to get a more precise description of these observables, Herwig was extended by a new soft model, namely the *post-hadronization momentum swapping* and its parameters were tuned to data. In this chapter, we discuss the mentioned observables, and the new model and its result in detail. This chapter is organized as follows: First the observables under consideration are introduced and we discuss default Herwig's ability to describe the data. In the following section, the basic idea of the new model is motivated. Subsequently, the algorithm is described. After that we tune the parameters of the model and other MPI-parameters to minimum bias observables and finally the results are shown.

## 5.1. Observables under Consideration

The considered data were measured by the ALICE [57] experiment at the center-of-mass energy $\sqrt{s} = 7$ TeV and were first published in [58]. These are two-particle correlations in the azimuthal angle $\phi$ of final-state particles, namely pions, kaons, protons and lambda-baryons, for (anti)meson-(anti)meson, meson-antimeson, (anti)baryon-(anti)baryon and baryon-antibaryon combinations in the pair. Here and in the following, particle-antiparticle pairings are referred to as opposite-sign pairings, while particle-particle pairings and antiparticle-antiparticle pairings are referred to as same-sign pairings.

The correlation $C(\Delta\phi)$ indicates whether the presence of a certain particle in an event reduces or increases the probability that another particle occurs at a certain angular distance $\Delta\phi$ from the first particle. Therefore, a background estimation by event-mixing is carried out.

The correlation function is integrated over rapidity and transverse momentum. The employed transverse momentum cut is $p_T \geq 0.5$ GeV and the rapidity-cut is $y \leq 0.8$, since the rapidity range of the measurement is limited by the architecture of the ALICE-detector. Additionally, only hadron-pairs with a rapidity-distance less than 1.3 are taken into account, i.e. $\Delta y \leq 1.3$.

In the analyses the angular-correlation function $C(\Delta\phi; HH')$ of two hadrons $HH'$ is determined by

$$C(\Delta\phi; HH') = \frac{2 \cdot N(\Delta\phi; HH')}{N(\Delta\phi; HH'_{\text{mix}}) + N(\Delta\phi; H_{\text{mix}}H')}, \qquad (5.1)$$

where $N(\Delta\phi; HH')$ is the number of $HH'$-hadron-pairs with angular distance in the azimuthal interval $\Delta\phi$. In the numerator, we consider hadron pairs with both hadrons from the same event, while the pairs in the denominator are created from event mixing. That means the denominator indicates the number of pairs that can be expected by chance purely through the general particle distribution. Thus, the following applies for different values of the correlation function $C(\Delta\phi; HH')$:

1.) For $\mathbf{C(\Delta\phi; HH') < 1.0}$ an anticorrelation is observed for the respective hadron-pair.

2.) For $\mathbf{C(\Delta\phi; HH') = 1.0}$ no correlation or anticorrelation is observed for the respective hadron-pair.

3.) For $\mathbf{C(\Delta\phi; HH') > 1.0}$ a correlation is observed for the respective hadron-pair.

Figure 5.1 shows a selections of the angular-correlations functions comparing the output of Herwig 7.2 (red line) with the measured data. For the runs, the baryonic colour reconnection model (see subsection 3.3.2.3) was applied and all model parameters were set to their default values. We use $K^+K^-$-pairs as an example for opposite-sign meson pairs and for same-sign meson pairs $K^-K^-$ and $K^+K^+$. For baryons, we use $p\bar{p}$-pairs and $p\Lambda$ and $\bar{p}\bar{\Lambda}$ respectively. Data for mesons and baryon-antibaryon pairs exhibit a peak for small angular distances. The Herwig output reproduces these small-distance peaks, but exceeds them.

Additionally, for baryon-antibaryon pairs a correlation for back-to-back particles is observed in the Herwig output, which is not supported by data. For baryon–baryon and antibaryon–antibaryon pairs, where both particles have the same baryon number, near-side anticorrelation structure arises in data, which is also reproduced by the Herwig output. It is reasonable to assume that the overly strong correlations are due to the hadronization model. In section 3.3.4 we described the pairwise cluster decay, which may induce correlations, especially in combination with the colour reconnection model. Due to colour reconnection nearby partons tend to be together in clusters and subsequently these near-side partons hadronize together. Figure 3.3 illustrates that in the pairwise decays no baryon-baryon and antibaryon-antibaryon pairs are produced. That might explain why the simulation does not exhibit a near-side peak for these pairs.

In the following subsections, we study the influence of colour reconnection, the proton remnant and the hadron decay model on the angular-correlations.
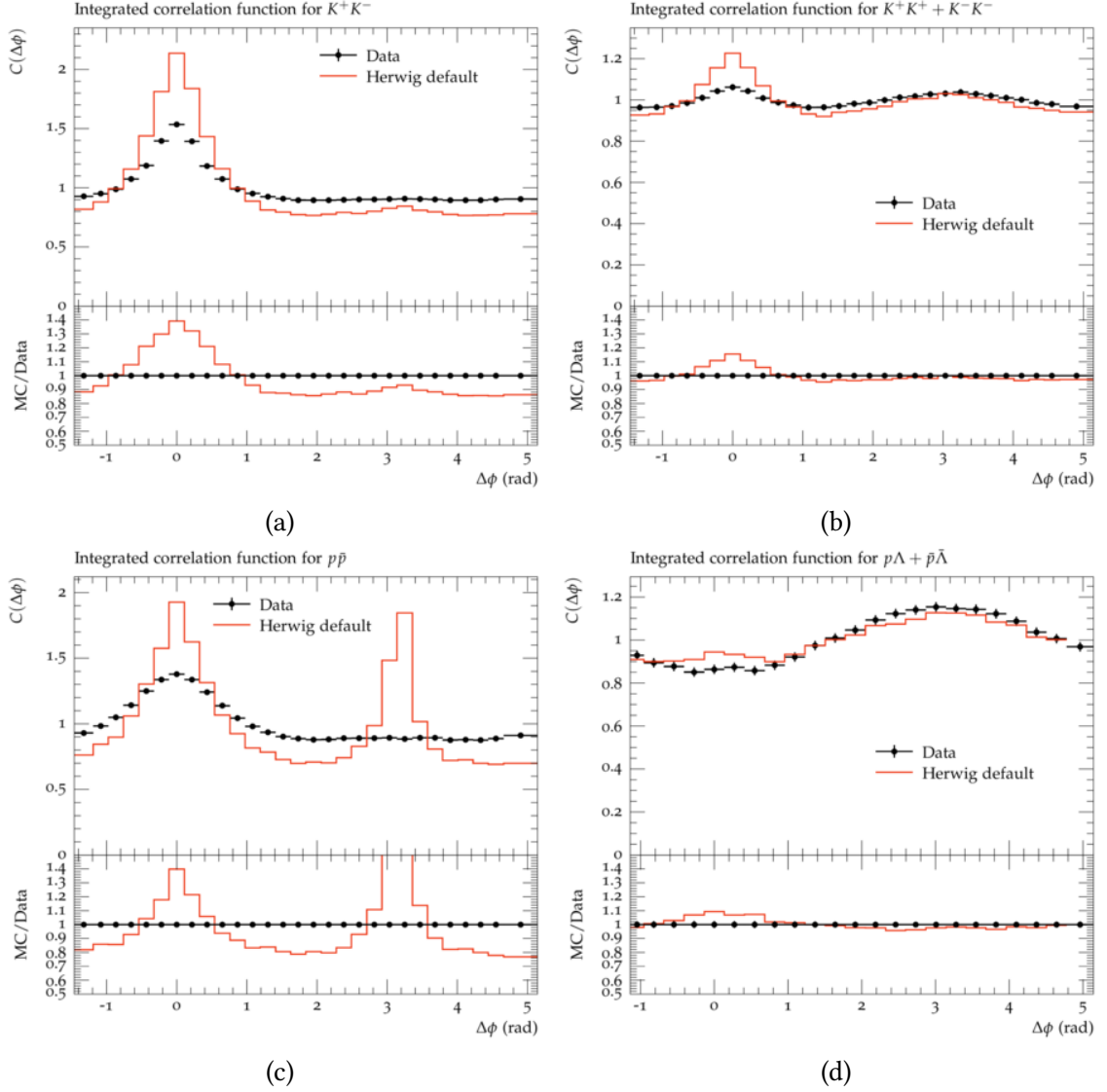
Figure 5.1.: Angular-correlation distributions for identified particles integrated over transverse momentum and rapidity measured by ALICE. The red line is the output of Herwig 7.2, where all model parameters are set to their default values. On display are the distributions for (a) same-sign kaon-pairs, (b) opposite-sign kaon-pairs, (c) same-sign proton-pairs and (d) opposite-sign proton-lambda-pairs.

### 5.1.1. Colour Reconnection

As indicated above, a strong association between colour reconnection and the observables under consideration is expected. The colour reconnection model has a significant impact on which partons hadronize together and how close they are in space and momentum. Hence, in figure 5.2 the Herwig output for different colour reconnection models is shown. The red line gives the output for no colour reconnection, i.e. the colour structure from the parton shower determines directly the composition of the cluster which either decay to hadrons directly or undergo the cluster fission process first. The blue line gives the output for only mesonic colour reconnection enabled, i.e. no baryonic clusters are produced in the colour reconnection process. Therefore, the baryonic colour reconnection model (see subsection 3.3.2.3) is applied with the baryonic reconnection probability set to 0 $p_B = 0$. The green line finally shows the output for baryonic and mesonic colour reconnection enabled with default parameter settings and thus, it is the same output as displayed in figure 5.1.

It can be observed that turning off the colour reconnection model causes a reduction of the near-side angular-correlations in the simulated data. In the case of $K^+K^-$-pairs, the simulation without colour reconnection reproduces the measured data accurately.

Applying mesonic colour reconnection increases the near-side correlation, while additional baryonic colour reconnection is associated with a decrease in these. Therefore, it might be assumed that a decrease of mesonic and an increase of baryonic colour reconnection would entail a more accurate description of these data. However, it should be noted that mesonic colour reconnection is of great importance for describing other important minimum bias observables accurately.

Subfigure 5.2d illustrates that colour reconnection also affects the near-side anticorrelations of baryon-baryon and antibaryon-antibaryon pairs. These anticorrelations are only reproduced if baryonic colour reconnection is enabled. Hence, it is reasonable to assume that particles originating from baryonic clusters lead to these.

### 5.1.2. Proton Remnants

At this point, we briefly highlight the influence of the proton remnants on the simulated data. In figure 5.3 the $p\bar{p}$-angular-correlation distribution for different particles is plotted. The red line shows the inclusive correlation distribution for all final state proton-antiproton pairs. The green line gives the distribution for proton-antiproton pairs where both hadrons originate from the remnants of the colliding protons. In contrast, the blue line is the distribution for all proton-antiproton pairs except those originating from remnants.

A strong back-to-back correlation for the remnant-particles is observed. Thus, the proton remnants appear to be of significant importance for the back-to-back-correlations not supported by the measured data. However, they do not seem to be the only source according to the blue line. This observation could be a starting point for future changes to Herwig aiming to improve the description of angular-correlations.
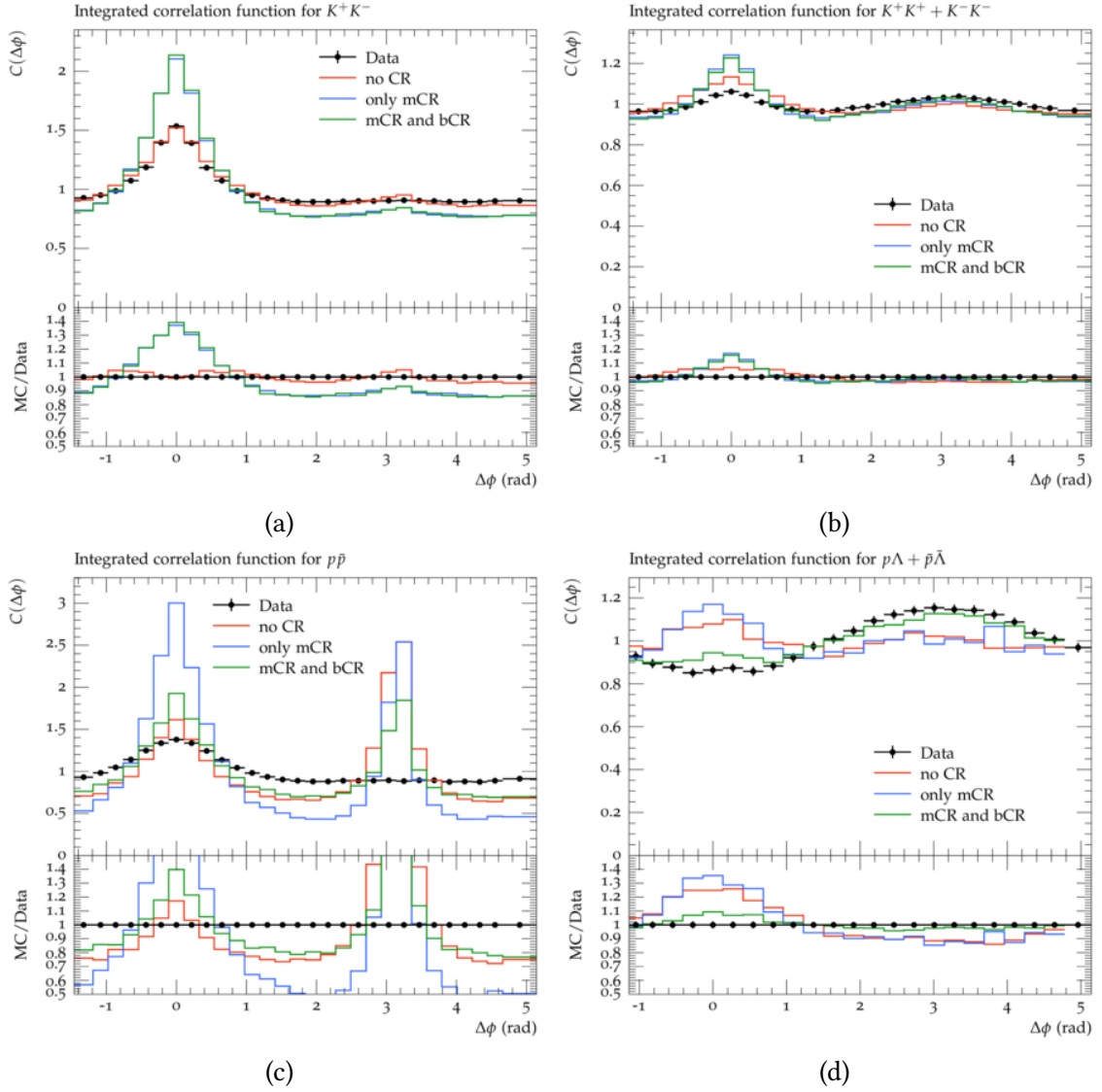
Figure 5.2.: Angular-correlations for different colour reconnection models. The red line is the Herwig output for no colour reconnection, the blue line for only mesonic colour reconnection and the green line for mesonic and baryonic colour reconnection. Strong near-side angular-correlations are associated with mesonic colour reconnection. Baryonic colour reconnection seems to be responsible for near-side anticorrelation.
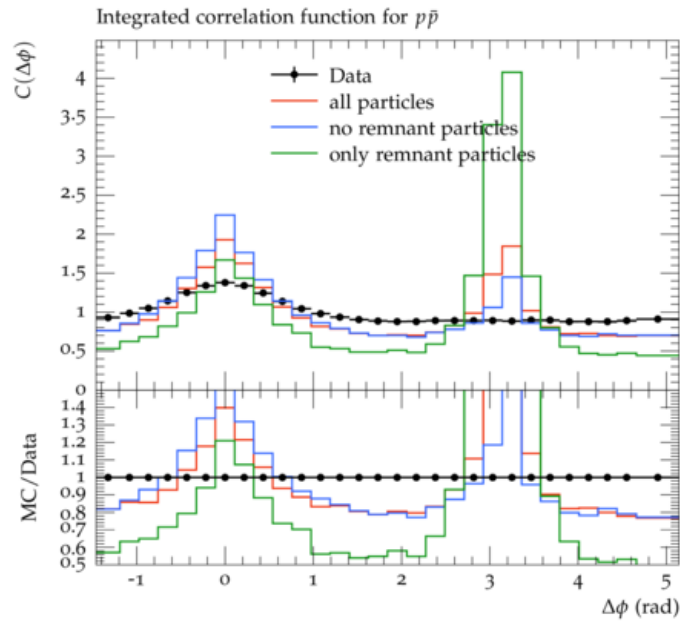
Figure 5.3.: Angular-correlation of particles originating from proton remnants (green line) and particles not originating from proton remnants (blue line). A strong back-to-back angular-correlation of opposite-sign baryon pairs originating from remnants is observed.

### 5.1.3. Hadron Decay

In addition to the actual hadronization process, the decay from excited hadrons originating from the cluster decays into the final state particles (see subsection 3.3.4) is a soft part of the event simulation. Therefore, it is interesting to investigate whether this has an influence on the considered correlations distributions. To get a first indication, Herwig runs were performed with hadron decays turned off. The distributions generated this way do not show major deviations from the previous ones. This suggests that the hadron decay model has no relevant influence on the considered observables. Corresponding plots are shown in appendix section B.1.

## 5.2. **Motivation and Fundamentals**

Above we observed that Herwig fails to describe angular-correlation in all detail. Furthermore we made the reasonable assumption that this is due to the cluster hadronization process in combination with the colour reconnection model. In order to improve the description of the considered observables, an obvious approach would be to make changes in these models. For instance, an alternative to cluster decay in two hadrons could be implemented. However, pairwise hadronization has the strength that momentum, energy and flavour conservation are baked into the prescription. Thus, replacing it would emerge various complex issues. Meanwhile colour reconnection is indispensable for the description of other minimium bias observables, for instance, the average transverse momentum over the charged multiplicity.

Therefore, we pursue a different and less complex approach. Instead of preventing the emergence of correlations in the hadronization process, we decorrelate the hadrons afterwards. The basic idea is to swap the momenta of pairs of excited hadrons, where the pairs are chosen randomly. This is expected to decorrelate the direction of the particles while other key observables are not influenced. Since we just swap the momenta and do not generate any new hadrons with new momenta, the charged multiplicity, transverse momentum and rapidity should remain statistically unchanged.

We name this new phenomenological model *post-hadronization momentum swapping*. In the following the corresponding algorithm is discussed in more detail.

At this point we notice briefly that in the Lund-String hadronization model [28] used by Pythia the so-called *popcorn* model plays an important role for reducing unwanted correlations. A detailed description of this model can be found in [27].

## 5.3. Algorithm

The starting point for the new model of post-hadronization momentum swapping is the excited hadrons emerging from the cluster decays. The momentum swapping algorithm then allows to decorrelate these hadrons by swapping their momenta pairwise. An overview of the workflow of the algorithm is shown in figure 5.4. The final algorithm for momentum swapping consists of the following steps:

1.) Initially the list of excited hadrons is shuffled. This is necessary, in order to prevent any bias that comes from the pairing of the hadrons considered for swapping.

2.) We pick the first two hadrons in the list and accept the swapping of their momenta with a certain probability $p_{\mathrm{swap}}$.

3.) If the swapping is accepted, it is carried out as follows. First, we boost the hadrons into their common center-of-mass frame. In this frame the hadrons are back-to-back and therefore, $\vec{p}_1 = -\vec{p}_2$ applies for their 3-momenta. This is crucial, in order to preserve both their energy and their invariant mass. Their 3-momenta are swapped and subsequently they are boosted back into the laboratory-frame.

4.) Repeat steps 2.) and 3.) for the next two hadrons in the list and so on until no or just one hadron is left.

The swapping-probability $p_{\mathrm{swap}}$ is a free parameter of the model. To be precise, there are three such parameters. The model is implemented in such a way that different probabilities can be set depending on the kind of hadrons considered for swapping. Hence, there is probability parameter for the case we consider two baryons $p_{\mathrm{swap}}^{\mathrm{bary}}$, one for the case we consider two mesons $p_{\mathrm{swap}}^{\mathrm{mes}}$ and finally one for the case we consider a meson and a baryon $p_{\mathrm{swap}}^{\mathrm{mes-bary}}$.

### 5.3.1. Hadrons originating from Baryonic Clusters

In section 5.1.1 we discovered that particles originating from baryonic clusters seem to be important for the correct description of the near-side anticorrelation of same-sign baryons. Considering this, it might be necessary to exclude the aforementioned baryons from the swapping procedure.

Hence, the model provides the boolean parameter `SwapParticlesfromBaryonicClusters`, which can be set by the user and determines, whether particles originating from baryonic clusters are considered for swapping or not. To implement this, it is crucial to identify these particles. The sketch in figure 5.5 illustrates the algorithm used for this identification. The fundamental idea is to go iteratively through the history of the considered hadron and check whether it contains a cluster with three components or not. If this is the case, the algorithm terminates and the particle is excluded from swapping. On the other hand, if we reach the parton-level history without finding such a cluster, the algorithm terminates and the particle is NOT excluded from swapping.
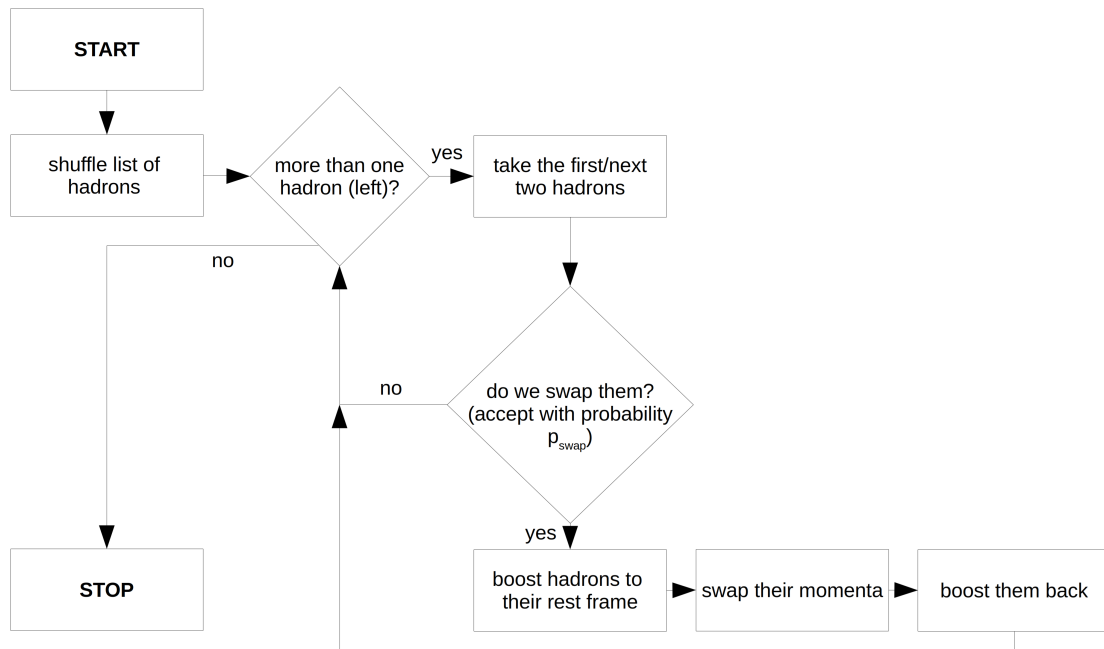
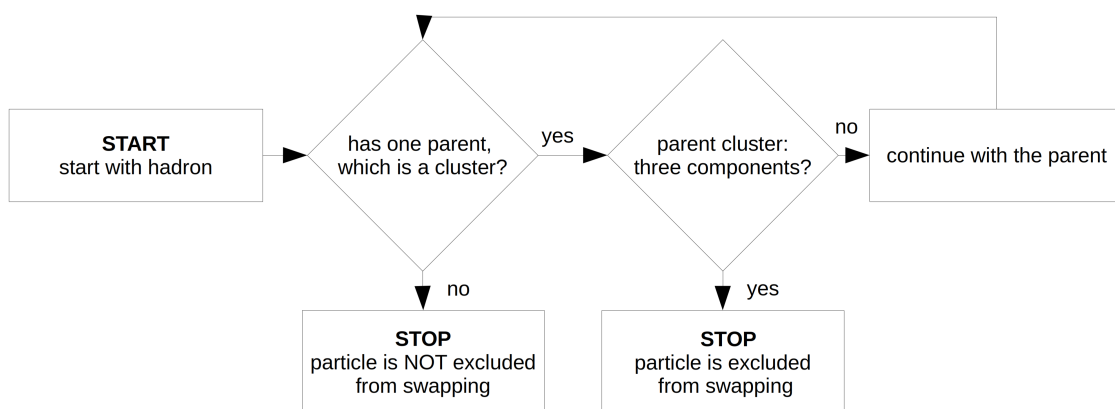Figure 5.4.: Sketch of the workflow of the post-hadronization momentum swapping model.



Figure 5.5.: Sketch of the algorithm to identify particles originating from baryonic clusters.

## 5.4. Validation and first Results

In order to validate that the implemented model reproduces the expected results, a set of angular-correlation distributions for different swapping probabilities is plotted in figure 5.6. The remaining can be found in the appendix section B.2. For the simulation exactly the same default settings were used as before and only the swapping model was additionally applied. Particles originating from baryonic clusters were excluded from swapping. Additionally, the different swapping probability parameters $p_{\text{swap}}^{\text{bary}}$, $p_{\text{swap}}^{\text{mes}}$ and $p_{\text{swap}}^{\text{mes−bary}}$ were all set to the same value, 0.5 or 1.0 respectively.

The description of data improves significantly for the $p\bar{p}$- and $K^+K^-$- pairs. The near-side correlation decreases and in case of the $p\bar{p}$ also the back-to-back-correlation is lowered. On the other hand, no such improvement is observed for the same-sign hadron-pairs. These distributions do not show any major changes.

However, the description of the near-side anticorrelation of same-sign baryon-pairs is neither affected strongly. Figure 5.7 illustrates the effect of swapping hadrons originating from baryonic clusters on the description of these anticorrelations. The blue line corresponds to a simulation with these hadrons included in momentum swapping, while the green line corresponds to a simulation with these hadrons excluded from swapping. Including particles originating from baryonic clusters in the swapping procedure causes a deterioration in the description of the near-side anticorrelation. Thus, it is reasonable to exclude them.

In summary, the swapping model entails a significant improvement in the description of angular-correlation, but is also limited.

### 5.4.1. Effect on other Minimum Bias Obsverbales

Above we assumed that the swapping model will not affect the output of minimum bias observables such as the charged multiplicities, the rapidity and the transverse momentum distributions. In fact this is confirmed for low-$p_T$ observables. However, for high-$p_T$ observables opposite observations are made. In figure 5.8 the charged $p_T$ distributions with swapping and without swapping for different swapping probabilities for $p_T > 100$ MeV and $p_T > 2500$ MeV are plotted. The data shown are from ATLAS [48].

For high-$p_T$ a significant deviation is observed. So far, the reason for this has not been further investigated. However, this might be due to the random choice of hadron pairs that are swapped. If we swap the momentum of two particles with medium transverse momentum, which are far in space and momentum, we may get one particle with high transverse momentum and one with low transverse momentum. And since before applying the swapping the percentage of high-$p_T$ hadrons is very low, this could lead to a shift towards high transverse momenta. Thus, this shift could perhaps be reduced, if the hadron pairs were selected according to a locality criterion. This could be an interesting aspect for further studies on the swapping model.
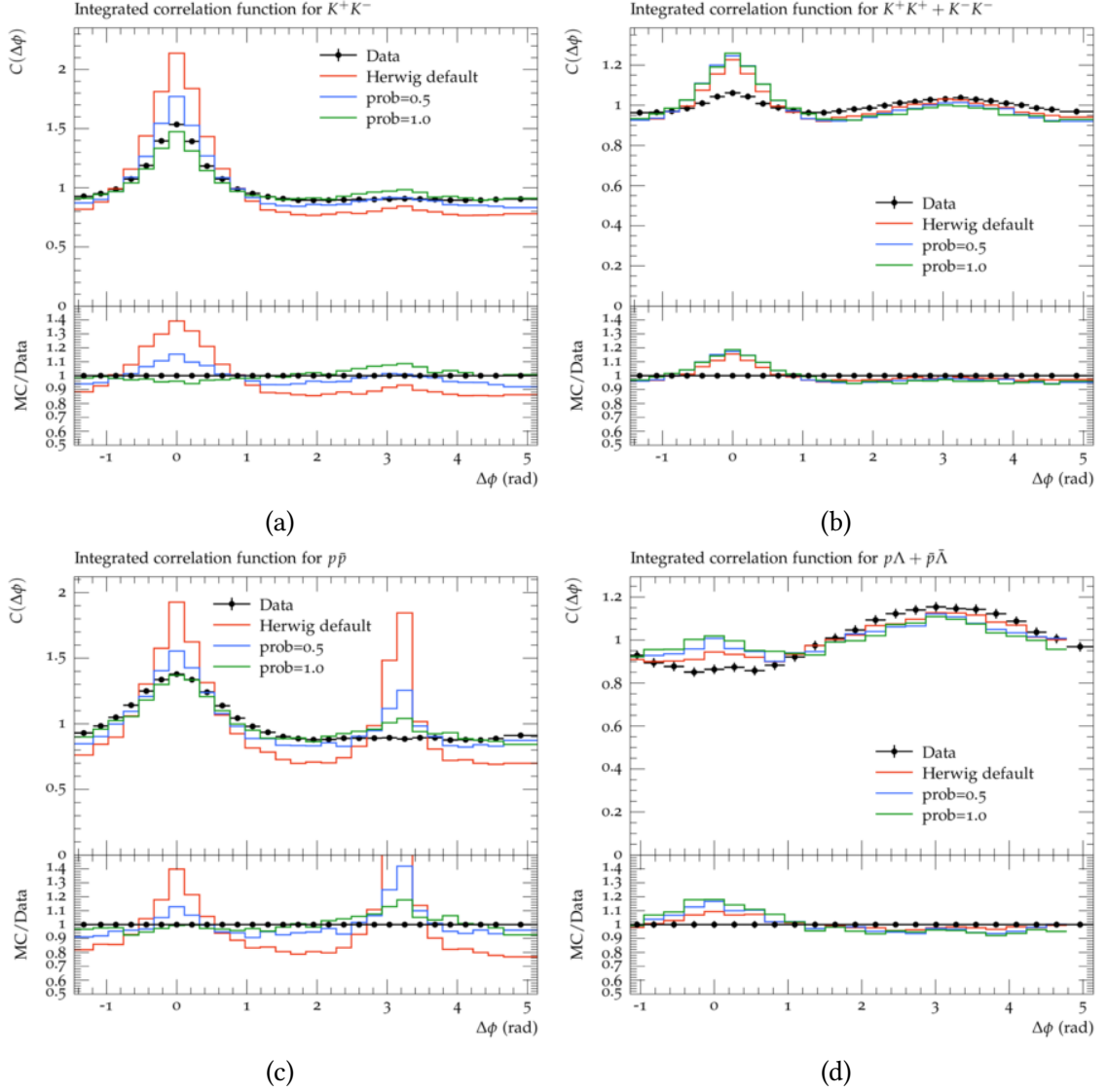
Figure 5.6.: Angular-correlations for different swapping probabilities. Particles originating from baryonic clusters are excluded from swapping. The red line shows the Herwig output with no post-hadronization momentum swapping model. The blue and the green line give the output for including swapping model, where the blue line is with swapping probability $p_{\text{swap}} = 0.5$ and the green line is with probability $p_{\text{swap}} = 1.0$.
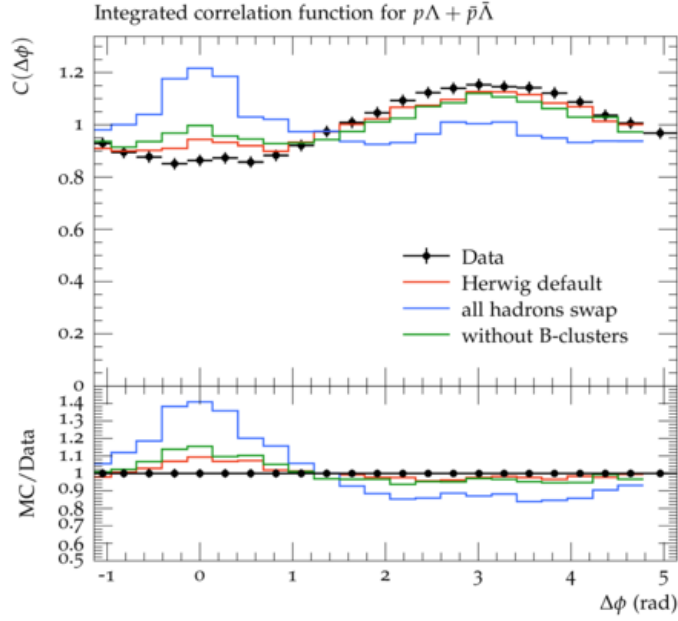
Figure 5.7.: $p\Lambda$- and $\bar{p}\bar{\Lambda}$- angular-correlation distributions for particles originating from baryonic clusters included (blue line) and not included (green line) in swapping. The swapping probability in both cases is set to $p_{\text{swap}} = 1.0$. The red line gives the Herwig output without the swapping model. Including particles originating from baryonic cluster in the swapping procedure causes a deterioration of the description of near-side anticorrelation.



(a)

(b)
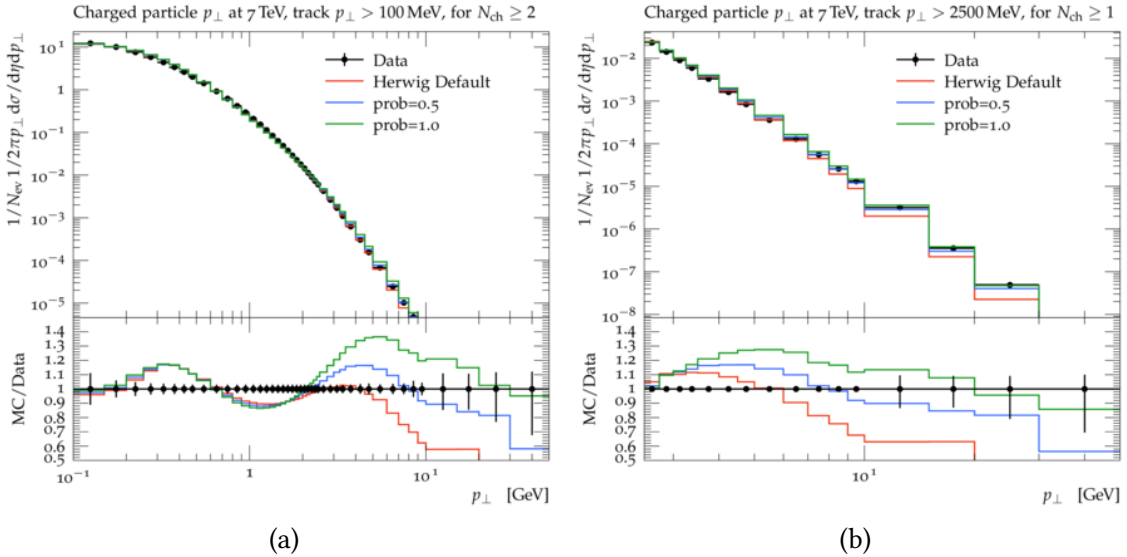
Figure 5.8.: Charged $p_T$-distributions with and without swapping for (a) $p_T > 100$ MeV and (b) $p_T > 2500$ MeV. For high-$p_T$ a significant deviation is observed.

## 5.5. **Tuning and Results**

The results presented above reveal that in order to achieve further improvements, aspects other than momentum swapping need to be considered as well. In section 5.1.1 we pointed out that colour reconnection impacts the angular-correlation-observables by a large degree. Additionally, one can observe that the observables are sensitive to other MPI-parameters. First and foremost $p_{T,0}^{\min}$ (see equation 3.24) and the inverse squared proton radius $\mu^2$ are to be mentioned. It seems natural to vary $p_{T,0}^{\min}$, $\mu^2$ and the colour reconnection parameters. However, such variations may entail changes in the description of other observables and thus, one is confronted with a complex optimization problem in a high-dimensional parameter space, where various observables have to be considered. Hence, it is reasonable to apply a generator tuning to constrain the value of the parameters.

The tuning is performed at $\sqrt{s}$ = 7 TeV center-of-mass energy and again by using the PROFESSOR tuning system [51] with AutoTunes [52]. Since particles from baryonic clusters have proven to be crucial for the description of the near-side anticorrelation of same-sign baryons, their swapping is disabled. The new baryonic-mesonic model (chapter 4) is used as colour reconnection model. We aim to obtain an adequate parameter choice for the combination of the two new models. A total of 11 parameters are tuned:

- the three momentum swapping probabilities: $p_{\text{swap}}^{\text{bary}}$, $p_{\text{swap}}^{\text{mes}}$ and $p_{\text{swap}}^{\text{mes}-\text{bary}}$

- the five probabilities of the baryonic-mesonic colour reconnection model: $p_{M,M}$, $p_{M,B}$, $p_{MB,MB}$, $p_{B,M}$ and $p_{B,B}$

- $p_{T,0}^{\min}$, parameter of the parameterisation of soft-hard-threshold transverse momentum in the MPI-model (see equation 3.24)

- the squared inverse proton radius $\mu^2$, which controls the matter distribution within the proton

- the ladder multiplicity factor $n_{\text{ladder}}$, a parameter of the soft part of the MPI-model

We decide to tune $n_{\text{ladder}}$, because it controls the number of soft gluons per rapidity. Thus, it may act as a counterbalance to $\mu^2$ and $p_{T,0}^{\min}$ with respect to particle multiplicity and result in more freedom in the variation of these parameters. The `StepFactor` of the colour reconnection model is not included in the tuning procedure and left at $f_{\text{step}}$ = 1.04.

We tune the parameters to the data on angular-correlation mentioned above and to minimum bias data measured by ATLAS [53], we used in section 4.3.

For some of the parameters the results are in a broad range and the tune does not converge at all. For that reason, these parameters are manually adjusted in order to obtain a good description of the data mentioned above. However, due to the large parameter space and high sensibility of various observables, that was immensely complicated. Moreover, it seems that angular-correlation observables "prefer" different values than the other minimum bias observables. We do not claim to have found the best values. The result can be regarded as a compromise. The preliminary final parameter choice based on tuning and fine-adjusting by hand is listed in table 5.1. They produce a satisfactory description of the considered observables. However, possibly future tunes may lead to further improvements.

Table 5.1.: Tuned and adjusted parameter values for the post-hadronization momentum swapping and baryonic-mesonic colour reconnection model. *Default* states the value used as a default in the current Herwig version and *range* gives the parameter range used for tuning.

| parameter | default | range | new value |
|:---:|:---:|:---:|:---:|
| $p_{T,0}^{\mathrm{min}}$ | 2.87 | $1.0 - 5.0$ | 4.98 |
| $\mu^2$ | 1.1 | $0.0 - 2.0$ | 2.1 |
| $n_{\mathrm{ladder}}$ | 0.6 | $0.0 - 2.0$ | 0.78 |
| $p_{M,M}$ | 0.95 [1] | $0.0 - 1.0$ | 0.01 |
| $p_{M,B}$ | 0.7 | $0.0 - 1.0$ | 0.98 |
| $p_{MB,MB}$ | None | $0.0 - 1.0$ | 0.33 |
| $p_{B,B}$ | None | $0.0 - 1.0$ | 0.19 |
| $p_{B,M}$ | None | $0.0 - 1.0$ | 0.01 |
| $p_{\mathrm{swap}}^{\mathrm{bary}}$ | None | $0.0 - 1.0$ | 0.39 |
| $p_{\mathrm{swap}}^{\mathrm{mes}}$ | None | $0.0 - 1.0$ | 0.99 |
| $p_{\mathrm{swap}}^{\mathrm{mes-bary}}$ | None | $0.0 - 1.0$ | 0.95 |

[1] To be exact, $p_{M,M}$ does not have a default value so far, since it is defined as the probability $3M \rightarrow 3M'$. What is given here is the default value for $2M \rightarrow 2M'$.

It is directly noticeable that the values for the MPI-parameters $p_{T,0}^{\mathrm{min}}$ and $\mu^2$ as well as for the mesonic colour reconnection probability $p_{M,M}$ differ strongly from their default values. For the angular-correlation observables, for which the results are plotted in figure 5.9, we achieve a significant improvement compared to the original Herwig output. The peak for back-to-back opposite-sign baryon pairs almost completely disappears. However, for the same-sign meson pairs, there is still no major change in the description recognized. Plots for further particle-pairs can be found in the appendix section B.2.

For the minimum bias observables from ATLAS the picture is mixed. For the charged transverse momentum distributions, we generally obtain an improved description. On the

other hand, for the charged multiplicity distributions the output of the Herwig default setting fits the data better than our tuned new models. A set of example plots can be found in figure 5.10.
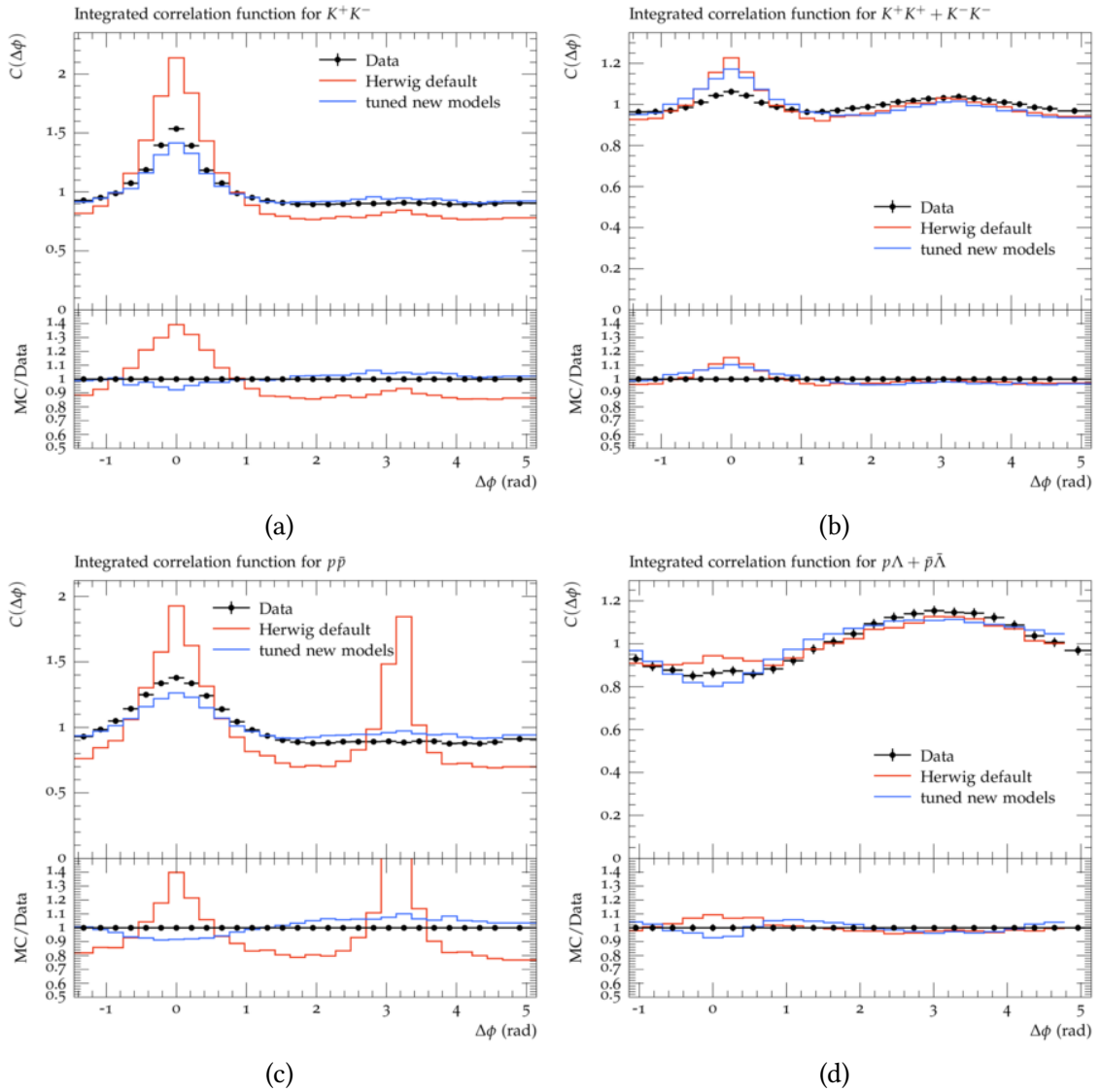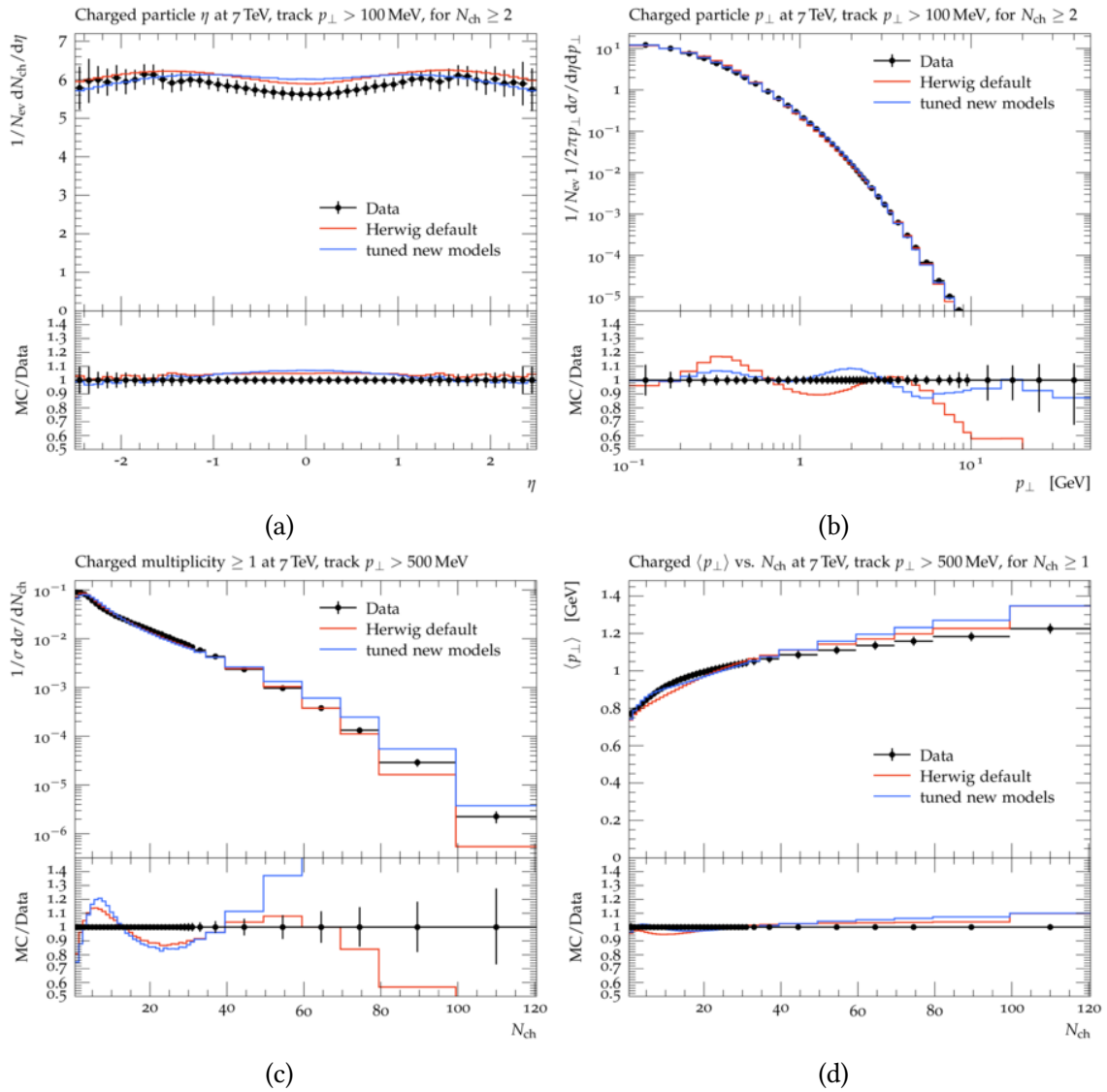


Figure 5.9.: Comparison of the default output of Herwig and the tune for new post-hadronization momentum swapping model in combination with the baryonic-mesonic colour reconnection model for angular-correlation distributions.

(a)

(b)

(c)

(d)

Figure 5.10.: Comparison of the default output of Herwig and the best tune for new post-hadronization momentum swapping model in combination with the baryonic-mesonic colour reconnection model for minimum bias data from ATLAS.

### 5.5.1. Results for identified Particle Yields

Next, we cross-check our tune with other observables which were not used for tuning. We make use of the transverse momentum distribution for kaons, pions and protons already considered when validating the baryonic-mesonic colour reconnection model (see subsection 4.3.3). The results are displayed in figure 5.11. We observe that the data are not described in a satisfactory way for the tuned model. Thus, it cannot be considered validated.

Here, it should be emphasized that these are the results for the tuned model, where colour reconnection and MPI-parameters deviate significantly from their default values. In order to check, whether the deviations are caused by the post-hadronization momentum swapping model directly, the results for default setting with additional post-hadronization momentum swapping (green line) are also plotted. It is observed that the model alone already causes changes in the description. This is also an interesting task for further studies in the future. However, the deviation can not be explained by the model only. Another reason may be the values of the MPI-model $\mu^2$ and $p_{T,0}^{\min}$, which deviate strongly from results of previous tunes. It seems that the description of the angular-correlation and other observables are in conflict with respect to these parameters.

## 5.6. Conclusion

We studied the description of angular-correlation distribution of identified particles, It was observed that the current version of Herwig fails to describe them accurately, especially because near-side correlations are overestimated.

We added a new phenomenological model, the post-hadronization momentum swapping, to Herwig aiming to decorrelate hadrons after the hadronization process. The model is at least able to improve the description of the considered observables. However, when tuning the model and MPI-parameters to data, we observed that the best parameter choice results in a significant deterioration in the description of other key-observables.

In the future, broader tunes including more observables may lead to improvement. However, potentially modification to the hadronization model could be expedient.
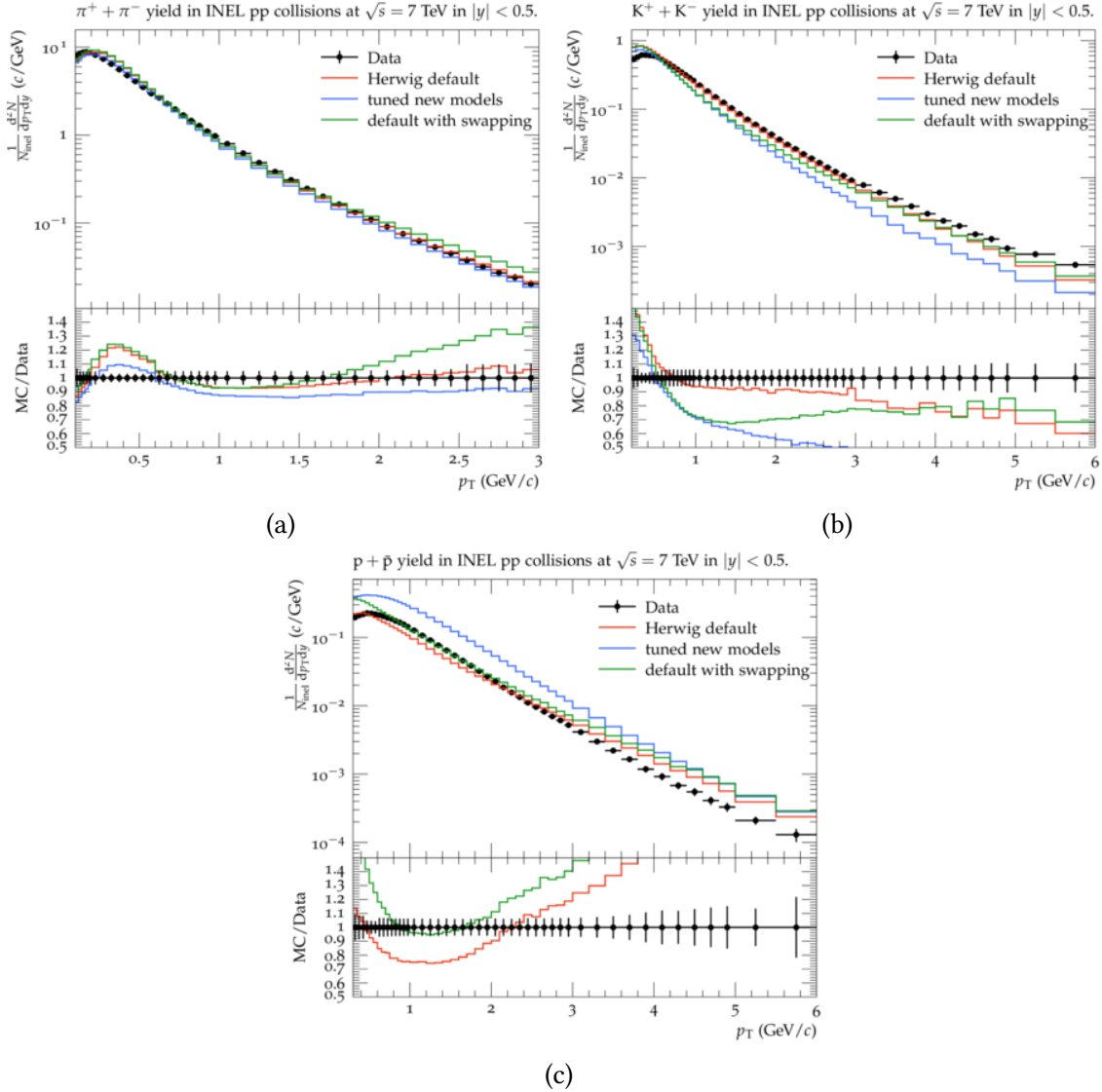
(a)

(b)



(c)

Figure 5.11.: Comparison of the default output of Herwig and the best tune for new post-hadronization momentum swapping model in combination with the baryonic-mesonic colour reconnection model for transverse momentum spectra of identified particles. The green line shows the results for Herwig default settings in combination with the post-hadronization momentum swapping, where the swapping probability is set to $p_{\mathrm{swap}} = 1.0$.

# 6.  Summary and Outlook

Within the framework of this thesis, a new colour reconnection model was implemented into Herwig. The new feature compared to the existing models is that the model allows baryonic clusters to be included in the reconnection process. The model parameters were tuned to minimum bias data and thus, a satisfactory description of data is achieved. So far, the tuning and analysing was performed only for $\sqrt{s} = 7$ TeV center-of-mass energy. One task of future studies is to cross-check the model for other energies, especially $\sqrt{s} = 13$ TeV. Additionally, it could be interesting to consider a wider range of observables in further tuning and analysing procedures. As an example we mention underlying event observables such as the charged particle density and the charged transverse momentum sum as a function of the leading track in jet events. Narrower tunes with focus on observables very sensitive to the model parameters are also a promising option. Through such further investigations, an even better parameter choice can probably be made, resulting in an even more accurate description and full validation of the model.

In the second part of this thesis, we considered and analysed the description of pairwise angular-correlations of identified particles, namely kaons, pions, protons and lambda-baryons, by Herwig. These are observables that have never been considered in detail by the Herwig project. We observed that the current Herwig version overestimates near-side correlations for meson pairs and baryon-antibaryon pairs and we made the assumption that this is due to the pairwise cluster decay implemented in Herwig. Additionally, the Herwig output exhibits a back-to-back peak for baryon-antibaryon pairs, which is not supported by data. We made the insight that the colour reconnection model has a significant impact on the description of these observables. Mesonic colour reconnection seems to contribute to the strong near-side correlations in a significant way, while particles originating from baryonic clusters produced through colour reconnection are essential for the description of near-side anti-correlations in antibaryon-antibaryon and baryon-baryon pairs.
In order to decorrelate the hadrons after the hadroniziation process, we introduced the post-hadronization momentum swapping model which pairwise swaps momenta of hadrons. The model provides the opportunity to exclude particles originating from baryonic clusters from swapping. First analyses showed that the new model entails an improvement of the description for at least some of the considered observables, while it leaves other key minimum bias observables unchanged - except for some high transverse momentum observables.
We tuned the parameter of the model as well as MPI- and colour reconnection parameters to the considered observables in combination with other minimum bias observables. Thus, a satisfactory or at least improved description of the tuned observables was obtained. However, the tuned parameter choice entails a significant deterioration in the description of the transverse momentum spectra of identified particles in minimum bias events. Thereby,

the large discrepancy in the value of the MPI-parameters compared to the results of previous tunes probably play a crucial role. We also observed that the post-hadronization momentum swapping model alone has impact on the description of these observables. The obtained results can not be seen as final.

However, the post-hadronization momentum swapping model achieves first promising successes and generally does what was anticipated from it. Future studies may entail further insights as well as improvement in its results and in the interaction with the rest of the simulation process. For one thing, it is interesting to investigate the reasons for the influence of the model on the high transverse momentum observables. In this context, it may be promising to introduce a criterion for the choice of the two respective hadrons which swap their momentum. Additional, further tunes incorporating different or more observables and perhaps more parameters of interest may lead to further improvements. However, it is also possible that the new model in combination with variation of model parameters in other parts of the simulation is not sufficient to gain a good description of the angular-correlations distributions. Hence, further model adjustment in Herwig may become necessary. A modification in the cluster hadronization process in such a way that the hadronization no longer is performed in pairs is expected to affect the output for the considered correlation observables by a large degree. Although this requires further physical considerations, since in the current model the pairwise decay provides a simple framework for ensuring energy and momentum conservation.

In general, the development of Monte Carlo event generators - and especially of the parts based on phenomenological modelling - is an ongoing process requiring constant adaptions and improvements, in order to meet the increasingly precise measurements and theoretical predictions.

# Bibliography

[1]   Manuel Bähr et al. "Herwig++ physics and manual". In: *The European Physical Journal C* 58.4 (Nov. 2008), pp. 639–707. ISSN: 1434-6052. DOI: `10.1140/epjc/s10052-008-0798-9`. URL: `http://dx.doi.org/10.1140/epjc/s10052-008-0798-9`.

[2]   Johannes Bellm et al. "Herwig 7.0/Herwig++ 3.0 release note". In: *The European Physical Journal C* 76.4 (Apr. 2016). ISSN: 1434-6052. DOI: `10.1140/epjc/s10052-016-4018-8`. URL: `http://dx.doi.org/10.1140/epjc/s10052-016-4018-8`.

[3]   Johannes Bellm et al. *Herwig 7.1 Release Note.* 2017. arXiv: `1705.06919` [`hep-ph`].

[4]   Johannes Bellm et al. "Herwig 7.2 release note". In: *The European Physical Journal C* 80.5 (May 2020). ISSN: 1434-6052. DOI: `10.1140/epjc/s10052-020-8011-x`. URL: `http://dx.doi.org/10.1140/epjc/s10052-020-8011-x`.

[5]   R. K. Ellis, W. J. Stirling, and B. R. Webber. *QCD and Collider Physics.* Cambridge Monographs on Particle Physics, Nuclear Physics and Cosmology. Cambridge University Press, 1996. DOI: `10.1017/CBO9780511628788`.

[6]   Richard P. Feynman. "The Behavior of Hadron Collisions at Extreme Energies". In: *Special Relativity and Quantum Theory: A Collection of Papers on the Poincaré Group.* Ed. by M. E. Noz and Y. S. Kim. Dordrecht: Springer Netherlands, 1988, pp. 289–30. ISBN: 978-94-009-3051-3. DOI: `10.1007/978-94-009-3051-3_25`. URL: `https://doi.org/10.1007/978-94-009-3051-3_25`.

[7]   David J. Gross and Frank Wilczek. "Ultraviolet Behavior of Nonabelian Gauge Theories". In: *Phys. Rev. Lett.* 30 (1973). Ed. by J. C. Taylor, pp. 1343–1346. DOI: `10.1103/PhysRevLett.30.1343`.

[8]   H. David Politzer. "Reliable Perturbative Results for Strong Interactions?" In: *Phys. Rev. Lett.* 30 (1973). Ed. by J. C. Taylor, pp. 1346–1349. DOI: `10.1103/PhysRevLett.30.1346`.

[9]   Particle Data Group et al. "Review of Particle Physics". In: *Progress of Theoretical and Experimental Physics* 2020.8 (Aug. 2020). 083C01. ISSN: 2050-3911. DOI: `10.1093/ptep/ptaa104`. eprint: `https://academic.oup.com/ptep/article-pdf/2020/8/083C01/34673722/ptaa104.pdf`. URL: `https://doi.org/10.1093/ptep/ptaa104`.

[10]  Gerard 't Hooft. "A Planar Diagram Theory for Strong Interactions". In: *Nucl. Phys. B* 72 (1974). Ed. by J. C. Taylor, p. 461. DOI: `10.1016/0550-3213(74)90154-0`.

[11]  Lyndon Evans and Philip Bryant. "LHC Machine". In: *Journal of Instrumentation* 3.08 (Aug. 2008), S08001–S08001. DOI: `10.1088/1748-0221/3/08/s08001`. URL: `https://doi.org/10.1088/1748-0221/3/08/s08001`.

[12]  Gavin Cullen et al. "Automated one-loop calculations with GoSam". In: *The European Physical Journal C* 72.3 (Mar. 2012). ISSN: 1434-6052. DOI: 10.1140/epjc/s10052-012-1889-1. URL: http://dx.doi.org/10.1140/epjc/s10052-012-1889-1.

[13]  Gavin Cullen et al. "GoSam-2.0: a tool for automated one-loop calculations within the Standard Model and beyond". In: *The European Physical Journal C* 74.8 (Aug. 2014). ISSN: 1434-6052. DOI: 10.1140/epjc/s10052-014-3001-5. URL: http://dx.doi.org/10.1140/epjc/s10052-014-3001-5.

[14]  Federico Buccioni et al. "OpenLoops 2". In: *The European Physical Journal C* 79.10 (Oct. 2019). ISSN: 1434-6052. DOI: 10.1140/epjc/s10052-019-7306-2. URL: http://dx.doi.org/10.1140/epjc/s10052-019-7306-2.

[15]  J. Baglio et al. *Release Note - VBFNLO 2.7.0*. 2014. arXiv: 1404.3940 [hep-ph].

[16]  K. Arnold et al. "Vbfnlo: A parton level Monte Carlo for processes with electroweak bosons". In: *Computer Physics Communications* 180.9 (Sept. 2009), pp. 1661–1670. ISSN: 0010-4655. DOI: 10.1016/j.cpc.2009.03.006. URL: http://dx.doi.org/10.1016/j.cpc.2009.03.006.

[17]  J. Baglio et al. *VBFNLO: A parton level Monte Carlo for processes with electroweak bosons – Manual for Version 2.7.0*. 2014. arXiv: 1107.4038 [hep-ph].

[18]  J. Alwall et al. "The automated computation of tree-level and next-to-leading order differential cross sections, and their matching to parton shower simulations". In: *JHEP* 07 (2014), p. 079. DOI: 10.1007/JHEP07(2014)079. arXiv: 1405.0301 [hep-ph].

[19]  Andy Buckley et al. "LHAPDF6: parton density access in the LHC precision era". In: *The European Physical Journal C* 75.3 (Mar. 2015). ISSN: 1434-6052. DOI: 10.1140/epjc/s10052-015-3318-8. URL: http://dx.doi.org/10.1140/epjc/s10052-015-3318-8.

[20]  Andy Buckley et al. "General-purpose event generators for LHC physics". In: *Physics Reports* 504.5 (July 2011), pp. 145–233. ISSN: 0370-1573. DOI: 10.1016/j.physrep.2011.03.005. URL: http://dx.doi.org/10.1016/j.physrep.2011.03.005.

[21]  V. N. Gribov and L. N. Lipatov. "Deep inelastic e p scattering in perturbation theory". In: *Sov. J. Nucl. Phys.* 15 (1972).

[22]  Guido Altarelli and G. Parisi. "Asymptotic Freedom in Parton Language". In: *Nucl. Phys. B* 126 (1977), pp. 298–318. DOI: 10.1016/0550-3213(77)90384-4.

[23]  Stefan Gieseke, Philip Stephens, and Bryan Webber. "New formalism for QCD parton showers". In: *Journal of High Energy Physics* 2003.12 (Dec. 2003), pp. 045–045. ISSN: 1029-8479. DOI: 10.1088/1126-6708/2003/12/045. URL: http://dx.doi.org/10.1088/1126-6708/2003/12/045.

[24]  Simon Plätzer and Stefan Gieseke. "Coherent parton showers with local recoils". In: *Journal of High Energy Physics* 2011.1 (Jan. 2011). ISSN: 1029-8479. DOI: 10.1007/jhep01(2011)024. URL: http://dx.doi.org/10.1007/JHEP01(2011)024.

[25]    Simon Plätzer and Stefan Gieseke. "Dipole showers and automated NLO matching in Herwig++". In: *The European Physical Journal C* 72.11 (Nov. 2012). ISSN: 1434-6052. DOI: 10.1140/epjc/s10052-012-2187-7. URL: http://dx.doi.org/10.1140/epjc/s10052-012-2187-7.

[26]    S. Catani and M.H. Seymour. "A general algorithm for calculating jet cross sections in NLO QCD". In: *Nuclear Physics B* 485.1-2 (Feb. 1997), pp. 291–419. ISSN: 0550-3213. DOI: 10.1016/s0550-3213(96)00589-5. URL: http://dx.doi.org/10.1016/S0550-3213(96)00589-5.

[27]    Torbjörn Sjöstrand, Stephen Mrenna, and Peter Skands. "PYTHIA 6.4 physics and manual". In: *Journal of High Energy Physics* 2006.05 (May 2006), pp. 026–026. ISSN: 1029-8479. DOI: 10.1088/1126-6708/2006/05/026. URL: http://dx.doi.org/10.1088/1126-6708/2006/05/026.

[28]    Bo Andersson et al. "Parton Fragmentation and String Dynamics". In: *Phys. Rept.* 97 (1983), pp. 31–145. DOI: 10.1016/0370-1573(83)90080-7.

[29]    B. R. Webber. "A QCD Model for Jet Fragmentation Including Soft Gluon Interference". In: *Nucl. Phys. B* 238 (1984), pp. 492–528. DOI: 10.1016/0550-3213(84)90333-X.

[30]    D. Amati and G. Veneziano. "Preconfinement as a Property of Perturbative QCD". In: *Phys. Lett. B83* 87 (1979). DOI: 10.1016/0370-2693(79)90896-7.

[31]    Stephen Wolfram. "Parton and Hadron Production in $e^+e^-$ Annihilation". In: *15th Rencontres de Moriond: Part I, High-Energy Hadronic Interactions.* 1980.

[32]    Geoffrey C. Fox and Stephen Wolfram. "A Model for Parton Showers in QCD". In: *Nucl. Phys. B* 168 (1980), pp. 285–295. DOI: 10.1016/0550-3213(80)90111-X.

[33]    Richard D. Field and Stephan Wolfram. "A QCD model for e+e- annihilations". In: *Nuclear Physics B* 213.1 (1983). ISSN: 0550-3213. DOI: https://doi.org/10.1016/0550-3213(83)90175-X.

[34]    Z. Koba, H. B. Nielsen, and P. Olesen. "Scaling of multiplicity distributions in high-energy hadron collisions". In: *Nucl. Phys. B40* (1972). DOI: 10.1016/0550-3213(72)90551-2.

[35]    S. Gieseke, C. Roehr, and A. Siodmok. "Colour reconnection in Herwig++". In: *The European Physical Journal C* 72 (2012). DOI: 10.1140/epjc/s10052-012-2225-5. arXiv: 1206.0041 [hep-ph].

[36]    Stefan Gieseke, Patrick Kirchgaeßer, and Simon Plätzer. "Baryon production from cluster hadronisation". In: *The European Physical Journal C* 78.2 (Feb. 2018). ISSN: 1434-6052. DOI: 10.1140/epjc/s10052-018-5585-7. URL: http://dx.doi.org/10.1140/epjc/s10052-018-5585-7.

[37]    Johannes Bellm et al. "Spacetime colour reconnection in Herwig 7". In: *The European Physical Journal C* 79.12 (Dec. 2019). ISSN: 1434-6052. DOI: 10.1140/epjc/s10052-019-7533-6. URL: http://dx.doi.org/10.1140/epjc/s10052-019-7533-6.

[38] Nicholas Metropolis et al. "Equation of State Calculations by Fast Computing Machines". In: *The Journal of Chemical Physics* 21.6 (1953), pp. 1087–1092. DOI: `http://dx.doi.org/10.1063/1.1699114`.

[39] David Grellscheid and Peter Richardson. *Simulation of Tau Decays in the Herwig++ Event Generator*. 2007. arXiv: `0710.1951 [hep-ph]`.

[40] Loyal Durand and Hong Pi. "High-energy nucleon-nucleus scattering and cosmic-ray cross sections". In: *Phys. Rev. D* 38 (1 July 1988), pp. 78–84. DOI: `10.1103/PhysRevD.38.78`. URL: `https://link.aps.org/doi/10.1103/PhysRevD.38.78`.

[41] Ivan Borozan and Michael Henry Seymour. "An eikonal model for multiparticle production in hadron-hadron interactions". In: *Journal of High Energy Physics* 2002.09 (Sept. 2002), pp. 015–015. DOI: `10.1088/1126-6708/2002/09/015`. URL: `https://doi.org/10.1088/1126-6708/2002/09/015`.

[42] Loyal Durand and Hong Pi. "Semihard QCD and high-energy pp and $\bar{p}p$ scattering". In: *Phys. Rev. D* 40 (5 Sept. 1989), pp. 1436–1445. DOI: `10.1103/PhysRevD.40.1436`. URL: `https://link.aps.org/doi/10.1103/PhysRevD.40.1436`.

[43] Manuel Bähr, Jonathan M Butterworth, and Michael H Seymour. "The underlying event and the total cross section from Tevatron to the LHC". In: *Journal of High Energy Physics* 2009.01 (Jan. 2009), pp. 065–065. DOI: `10.1088/1126-6708/2009/01/065`. URL: `https://doi.org/10.1088/1126-6708/2009/01/065`.

[44] S. Gieseke, P. Kirchgaesser, and F. Loshaj. "A New Model for Soft Interactions in Herwig". In: *Acta Physica Polonica B* 48.6 (2017), p. 1025. ISSN: 1509-5770. DOI: `10.5506/aphyspolb.48.1025`. arXiv: `1704.00911 [hep-ph]`. URL: `http://dx.doi.org/10.5506/APhysPolB.48.1025`.

[45] Johannes Bellm, Stefan Gieseke, and Patrick Kirchgaeßer. "Improving the description of multiple interactions in Herwig". In: *The European Physical Journal C* 80.5 (May 2020). ISSN: 1434-6052. DOI: `10.1140/epjc/s10052-020-8002-y`. arXiv: `1911.13149 [hep-ph]`. URL: `http://dx.doi.org/10.1140/epjc/s10052-020-8002-y`.

[46] Stefan Gieseke, Frasher Loshaj, and Miroslav Myska. *Towards Diffraction in Herwig*. 2016. arXiv: `1602.04690 [hep-ph]`.

[47] Stefan Gieseke, Frashër Loshaj, and Patrick Kirchgaeßer. "Soft and diffractive scattering with the cluster model in Herwig". In: *The European Physical Journal C* 77.3 (Mar. 2017). ISSN: 1434-6052. DOI: `10.1140/epjc/s10052-017-4727-7`. URL: `http://dx.doi.org/10.1140/epjc/s10052-017-4727-7`.

[48] G Aad et al. "Charged-particle multiplicities inppinteractions measured with the ATLAS detector at the LHC". In: *New Journal of Physics* 13.5 (May 2011), p. 053033. ISSN: 1367-2630. DOI: `10.1088/1367-2630/13/5/053033`. URL: `http://dx.doi.org/10.1088/1367-2630/13/5/053033`.

[49] David Sudermann. *Colour Reconnection in Herwig*. Masterthesis at KIT. Karlsruhe, Germany, 2019.

[50]   Andy Buckley et al. "Rivet user manual". In: *Computer Physics Communications* 184.12 (Dec. 2013), pp. 2803–2819. ISSN: 0010-4655. DOI: `10.1016/j.cpc.2013.05.021`. URL: `http://dx.doi.org/10.1016/j.cpc.2013.05.021`.

[51]   Andy Buckley et al. "Systematic event generator tuning for the LHC". In: *The European Physical Journal C* 65.1-2 (Nov. 2009), pp. 331–357. ISSN: 1434-6052. DOI: `10.1140/epjc/s10052-009-1196-7`. URL: `http://dx.doi.org/10.1140/epjc/s10052-009-1196-7`.

[52]   Johannes Bellm and Leif Gellersen. "High dimensional parameter tuning for event generators". In: *The European Physical Journal C* 80.1 (Jan. 2020). ISSN: 1434-6052. DOI: `10.1140/epjc/s10052-019-7579-5`. URL: `http://dx.doi.org/10.1140/epjc/s10052-019-7579-5`.

[53]   G. Aad et al. "The ATLAS Experiment at the CERN Large Hadron Collider". In: *JINST* 3 (2008), S08003. DOI: `10.1088/1748-0221/3/08/S08003`.

[54]   J. Adam et al. "Measurement of pion, kaon and proton production in proton–proton collisions at $\sqrt{s} = 7$ TeV". In: *The European Physical Journal C* 75.5 (May 2015). ISSN: 1434-6052. DOI: `10.1140/epjc/s10052-015-3422-9`. URL: `http://dx.doi.org/10.1140/epjc/s10052-015-3422-9`.

[55]   K. Aamodt et al. "Charged-particle multiplicity measurement in proton–proton collisions at $\sqrt{s} = 7$ TeV with ALICE at LHC". In: *The European Physical Journal C* 68.3-4 (June 2010), pp. 345–354. ISSN: 1434-6052. DOI: `10.1140/epjc/s10052-010-1350-2`. URL: `http://dx.doi.org/10.1140/epjc/s10052-010-1350-2`.

[56]   G. Aad et al. "Rapidity gap cross sections measured with the ATLAS detector in pp collisions at $\sqrt{s} = 7$ TeV". In: *The European Physical Journal C* 72.3 (Mar. 2012). ISSN: 1434-6052. DOI: `10.1140/epjc/s10052-012-1926-0`. URL: `http://dx.doi.org/10.1140/epjc/s10052-012-1926-0`.

[57]   K. Aamodt et al. "The ALICE experiment at the CERN LHC". In: *JINST* 3 (2008), S08002. DOI: `10.1088/1748-0221/3/08/S08002`.

[58]   Jaroslav Adam et al. "Insight into particle production mechanisms via angular correlations of identified particles in pp collisions at $\sqrt{s} = 7$ TeV". In: *Eur. Phys. J. C* 77.8 (2017). [Erratum: Eur.Phys.J.C 79, 998 (2019)], p. 569. DOI: `10.1140/epjc/s10052-017-5129-6`. arXiv: `1612.08975 [nucl-ex]`.

# A. Further Results of Baryonic-Mesonic Colour Reconnection

## A.1. Minimum Bias Observables

Here we show the remaining results for the minimum bias observables from ATLAS [48], which were used for the tuning of the baryonic-mesonic colour reconnection model.
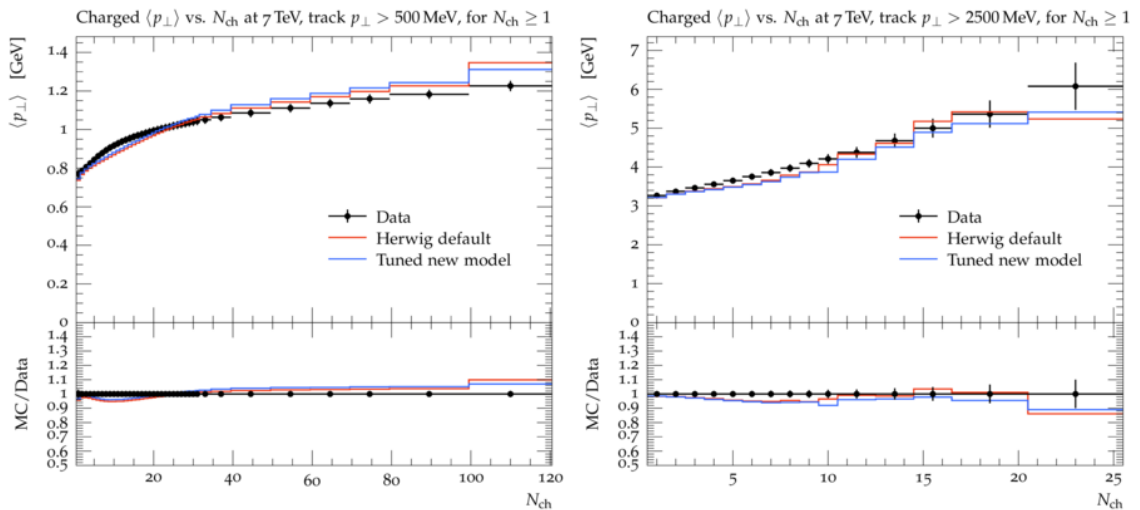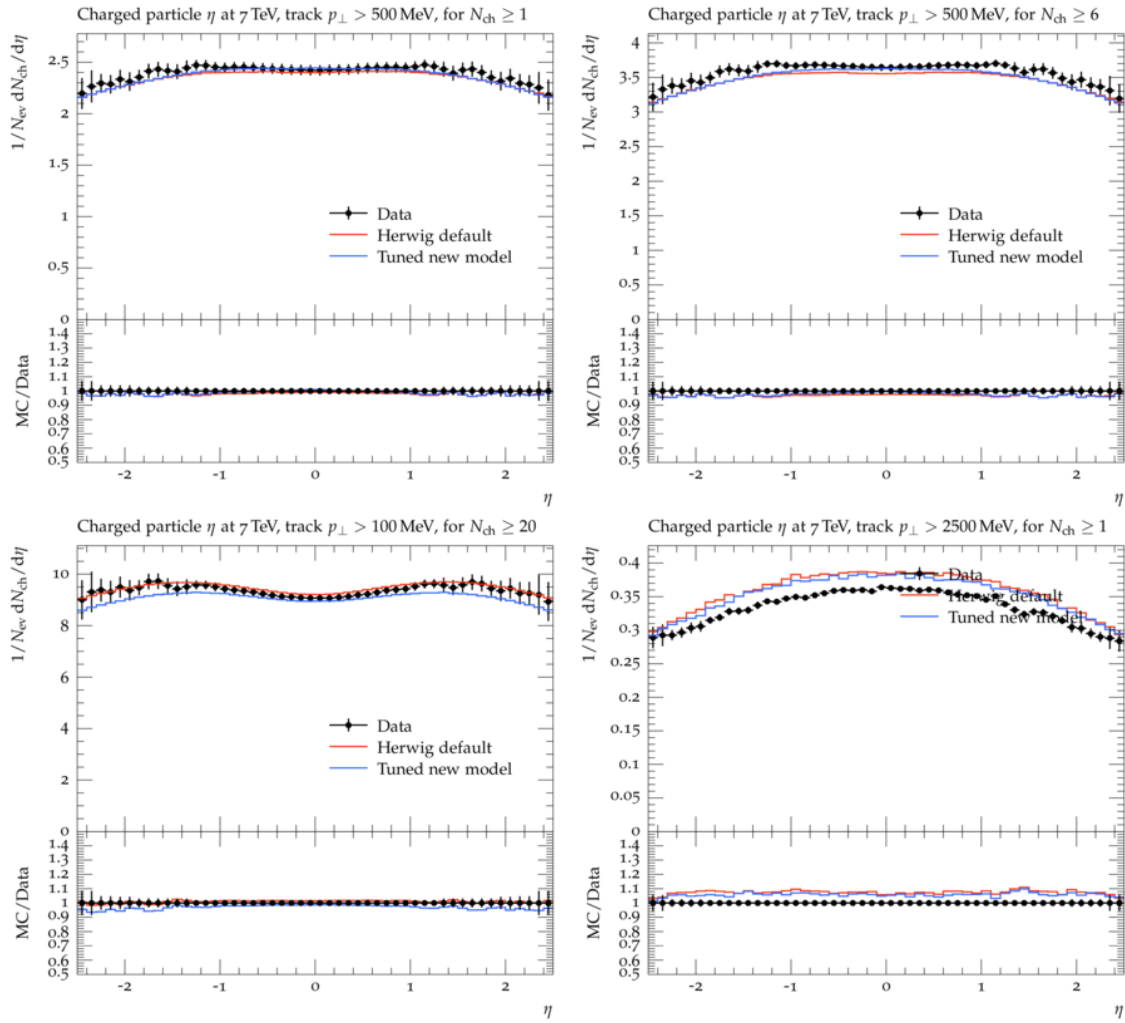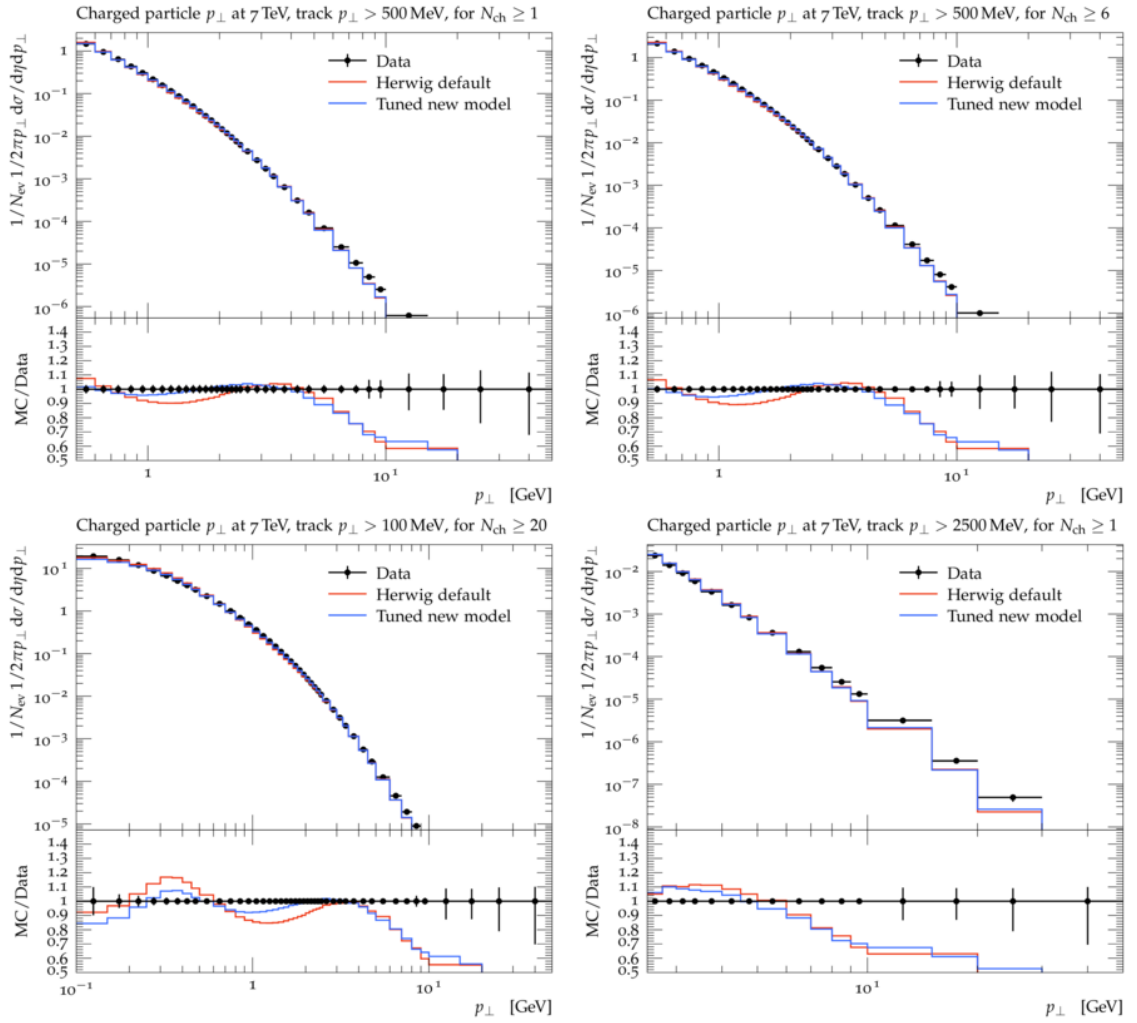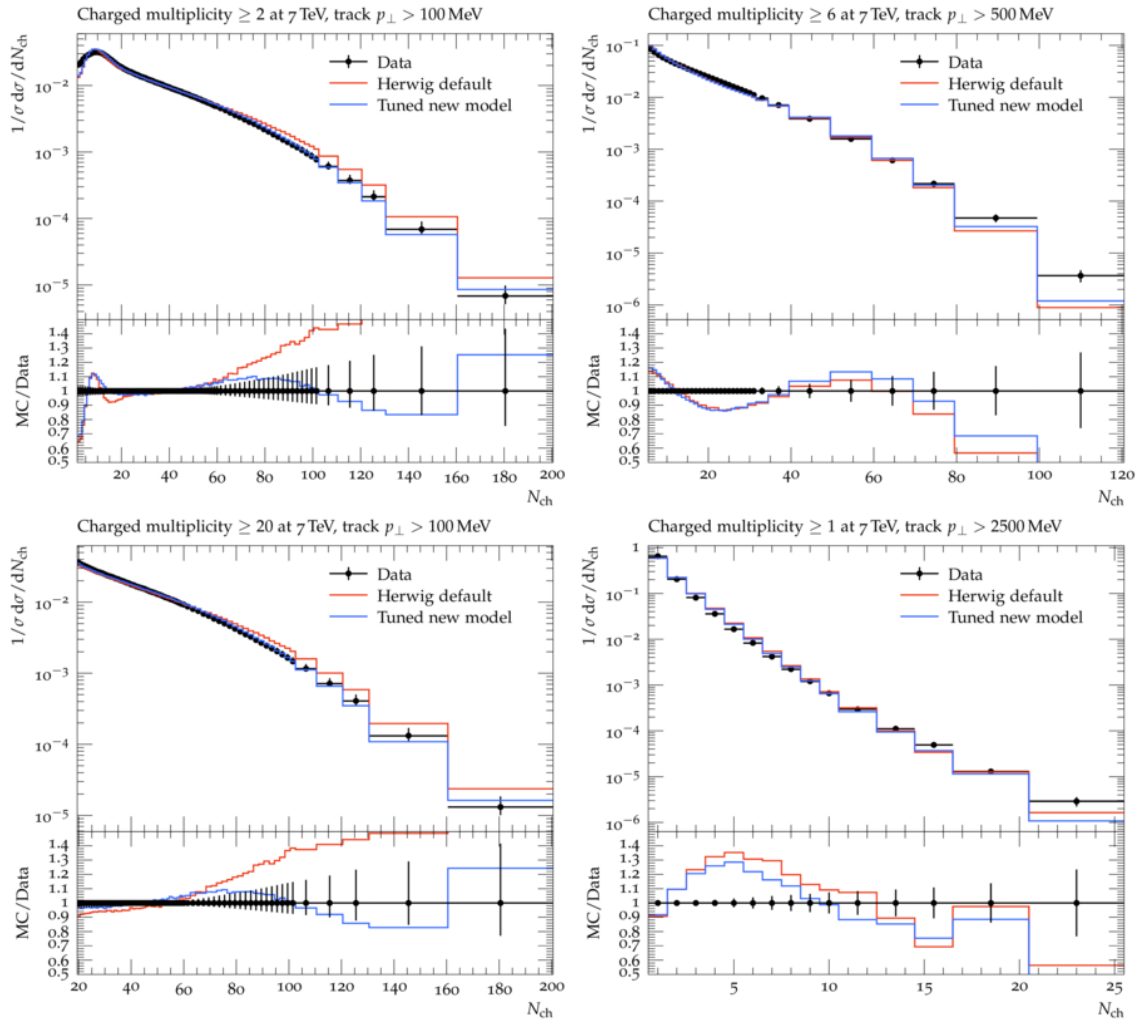


Figure A.1.: Comparison of the default output of Herwig and the best tune for the new baryonic-mesonic colour reconnection model for various averaged charged transverse momentum over charged multiplicity distributions. The data are measured by ATLAS and were used for tuning.
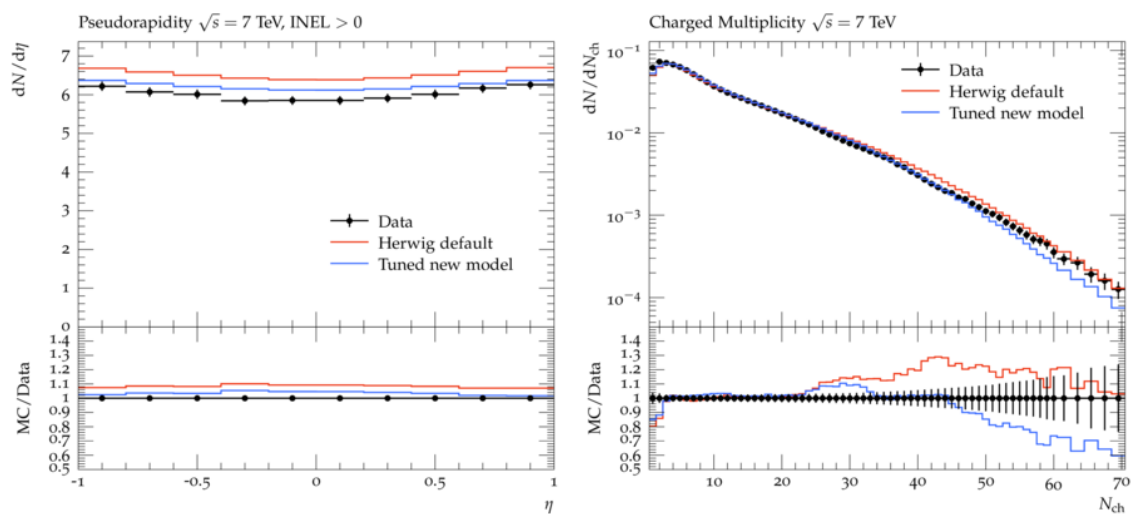
Figure A.2.: Comparison of the default output of Herwig and the best tune for the new baryonic-mesonic colour reconnection model for various charged rapidity distributions. The data are measured by ATLAS and were used for tuning.
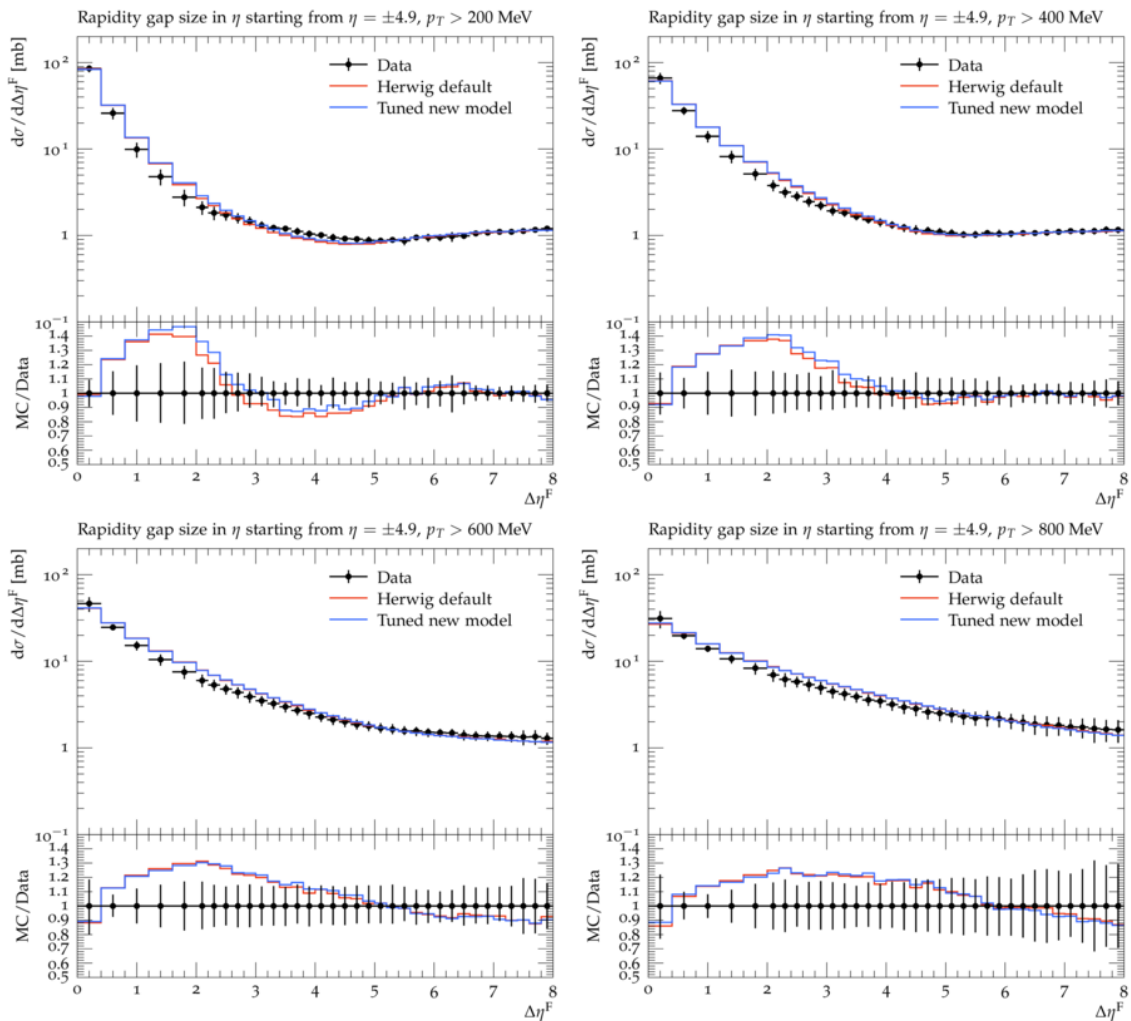
Figure A.3.: Comparison of the default output of Herwig and the best tune for the new baryonic-mesonic colour reconnection model for various charged transverse momentum distributions. The data are measured by ATLAS and were used for tuning.

Figure A.4.: Comparison of the default output of Herwig and the best tune for the new baryonic-mesonic colour reconnection model for various charged multiplicity distributions. The data are measured by ATLAS and were used for tuning.

## A.2. Pseudorapidity and Charged Multiplicity



Figure A.5.: Comparison of the default output of Herwig and the best tune for the new baryonic-mesonic colour reconnection model for pseudorapidity and charged multiplicity distributions. The data are measured by ALICE [55] and were NOT used for tuning.

## A.3. Rapidity Gap



Figure A.6.: Comparison of the default output of Herwig and the best tune for the new baryonic-mesonic colour reconnection model for rapidity gap cross sections. The data are measured by ATLAS [56] and were NOT used for tuning.

# B. Further Results for Post-Hadronization Momentum Swapping

## B.1. Disabled Decay Model
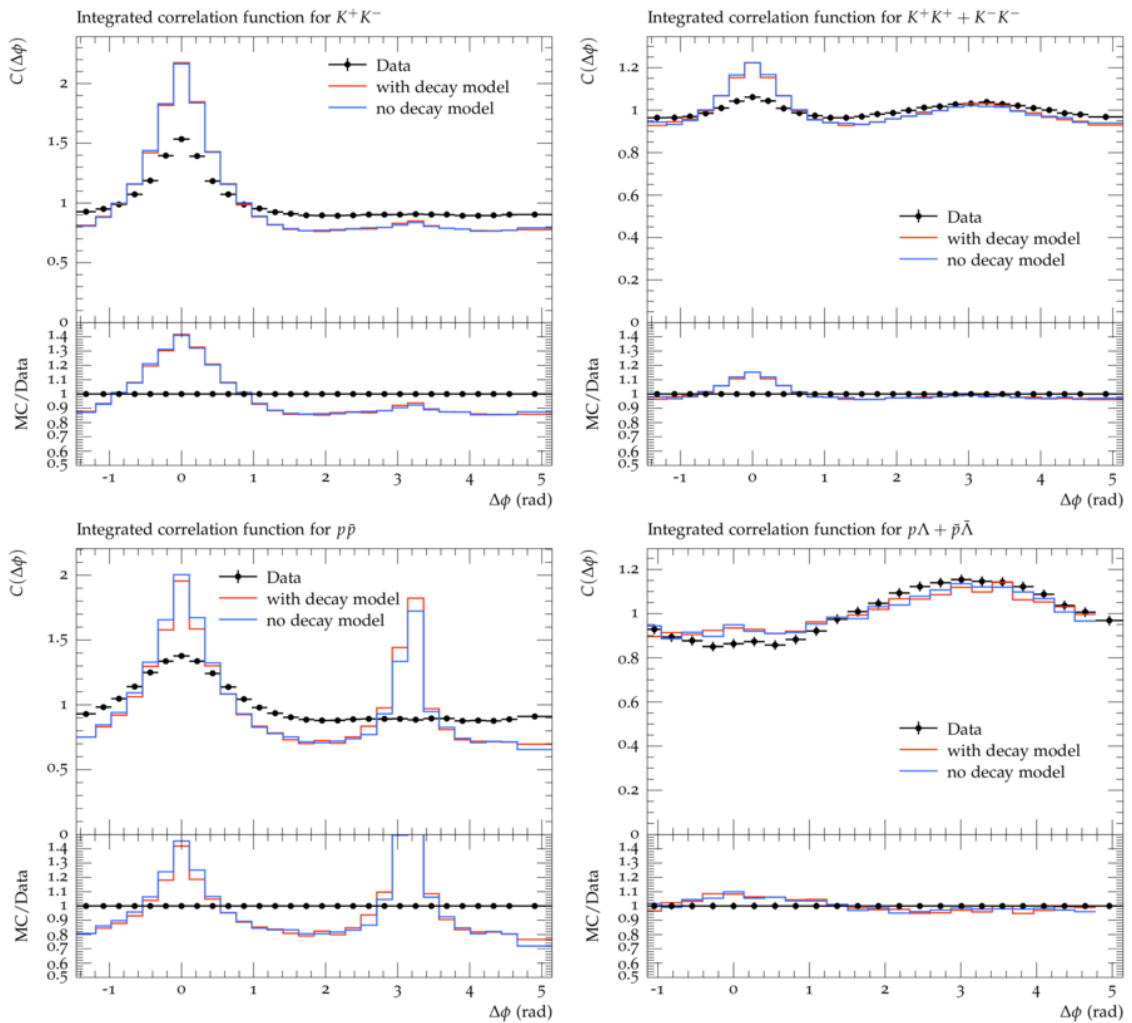


Figure B.1.: Angular-correlations for enabled (red line) and disabled (blue line) decay model. No major deviations are observed. This indicates that the hadron decay model in Herwig has no significant influence on the description of angular-correlation distributions. The data are measured by ALICE [58].

## B.2. Different Swapping Probabilities

Here, we show the remaining angular-correlation distributions for Herwig default settings without and with applied post-hadronization momentum swapping model. The data are measured by ALICE [58].
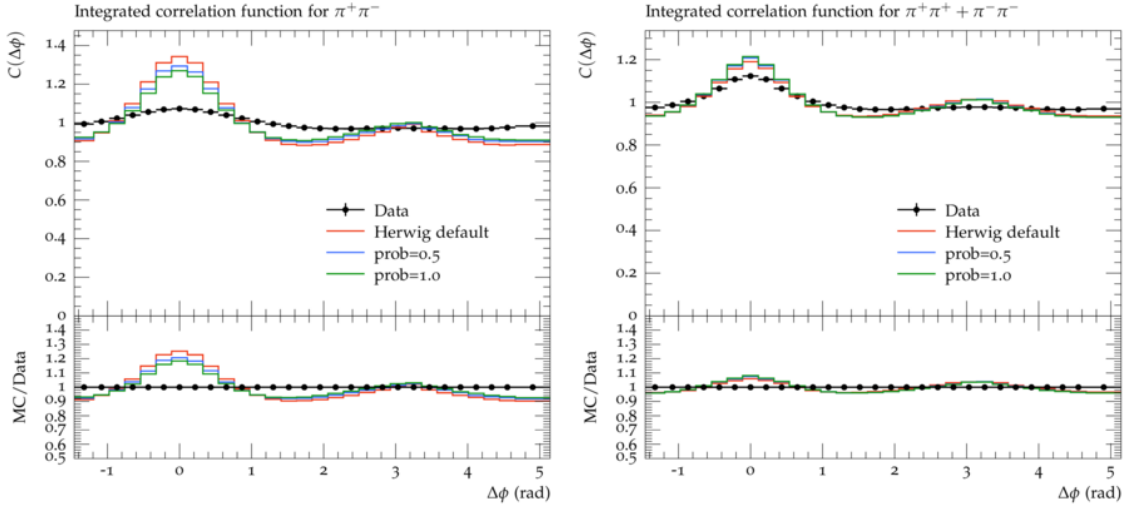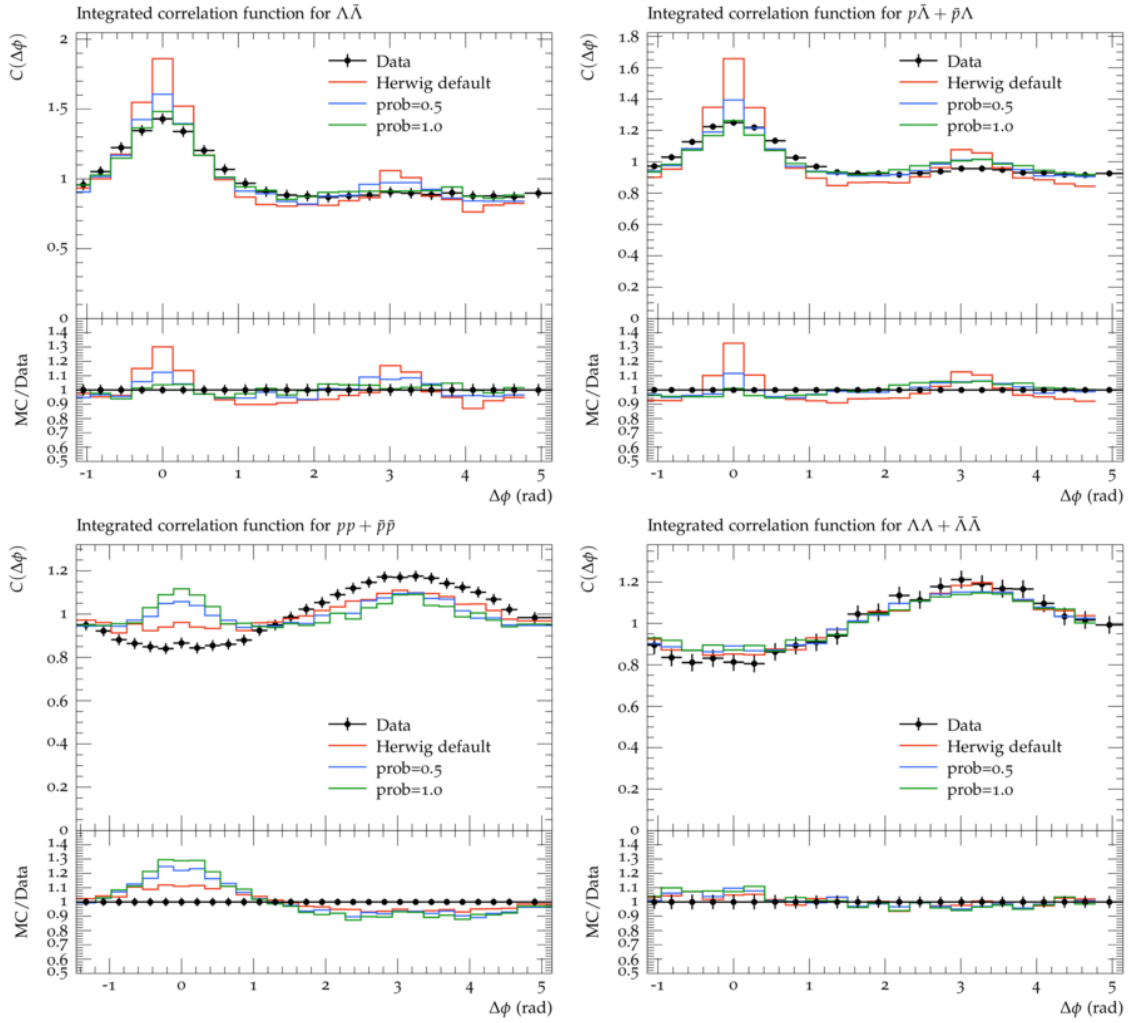


Figure B.2.: Angular-correlations of mesonic particle pairs for different swapping probabilities. Particles originating from baryonic clusters are excluded from swapping. The red line shows the Herwig output with disabled post-hadronization momentum swapping model. The blue and the green line give the output for applied swapping model, for the blue line with swapping probability $p_{\mathrm{swap}} = 0.5$ and for the green line with probability $p_{\mathrm{swap}} = 1.0$.

Figure B.3.: Angular-correlations of baryonic particle pairs for different swapping probabilities. Particles originating from baryonic clusters are excluded from swapping. The red line shows the Herwig output with disabled post-hadronization momentum swapping model. The blue and the green line give the output for applied swapping model, for the blue line with swapping probability $p_{\mathrm{swap}} = 0.5$ and for the green line with probability $p_{\mathrm{swap}} = 1.0$.

## B.3. Tuned Model

Here, we show the remaining angular-correlation distributions for the tuned post-hadronization swapping model in combination with the new baryonic-mesonic colour reconnection model and compare them with the distributions produced for Herwig default settings. The data are measured by ALICE [58].
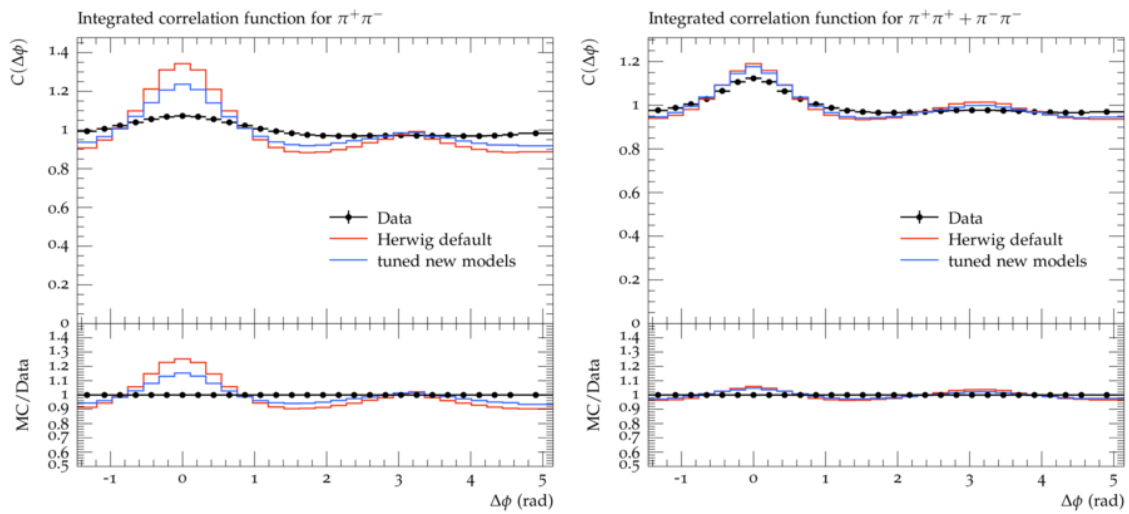


Figure B.4.: Comparison of the default output of Herwig and the tune for new post-hadronization momentum swapping model in combination with the baryonic-mesonic colour reconnection model for angular-correlation distributions of mesonic particle pairs.
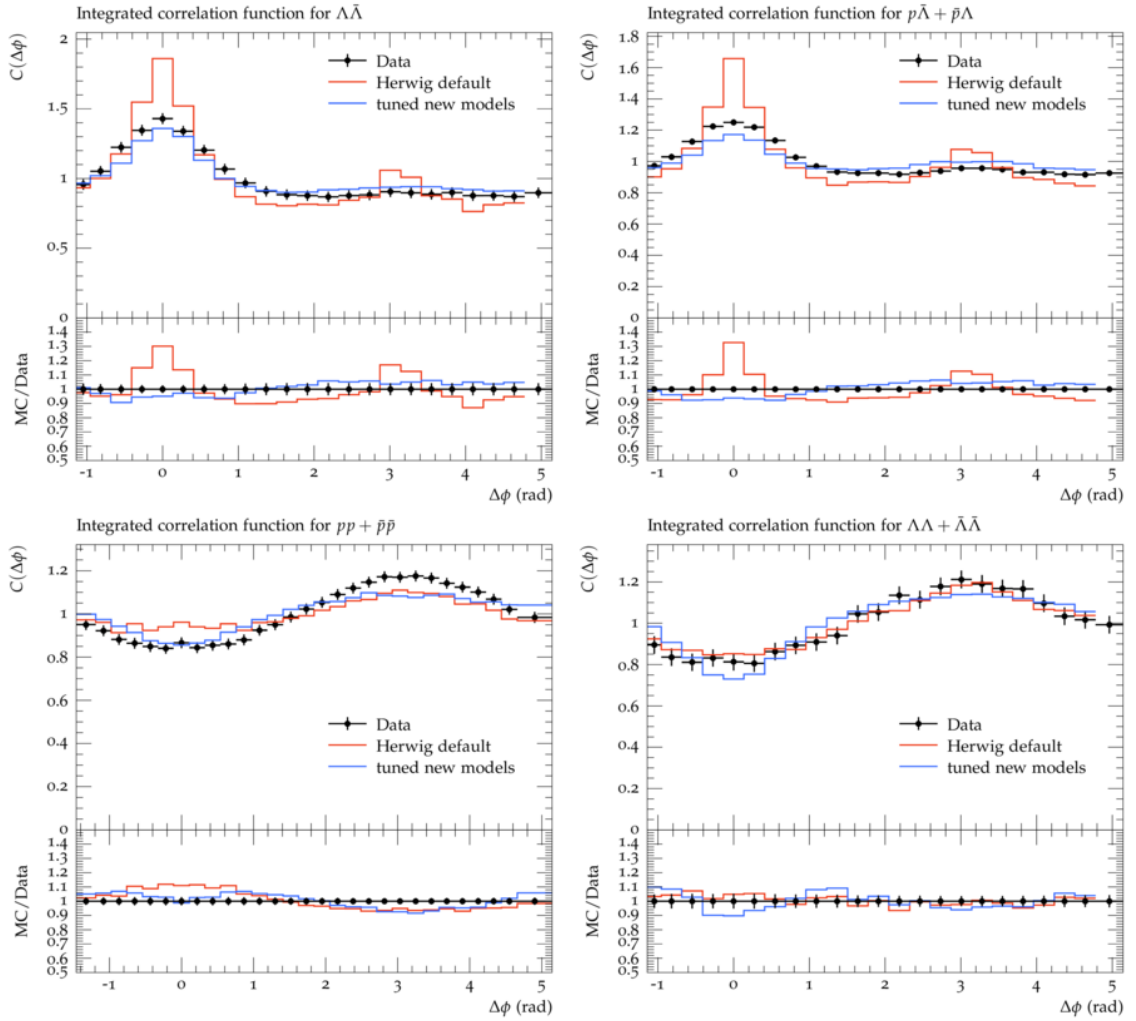
Figure B.5.: Comparison of the default output of Herwig and the tune for new post-hadronization momentum swapping model in combination with the baryonic-mesonic colour reconnection model for angular-correlation distributions of baryonic particle pairs.

# Acknowledgements

First of all, I want to thank my supervisor PD. Dr. Stefan Gieseke for giving me the opportunity for this thesis and working on this interesting topic. Moreover, I would like to thank him for his support during the whole time, the various meetings and discussions and the helpful answers to all my arising questions.

I would like to thank Prof. Dr. Gudrun Heinrich for agreeing to be the second reviewer of this thesis.

Next, I would like to thank Dr. Cody Duncan for proofreading the whole thesis and also for his open ear to all my questions.

Another thanks goes to Dr. Patrick Kirchgaesser for many times he gave me advice throughout the thesis.

Moreover, I thank Julian Lukwata who helped me a lot when I had problems to understand the software architecture of Herwig - especially in the first months of my work. And also for accompanying me almost the whole time of my studies in Karlsruhe.

Thanks to all members of the Institute of Theoretical Physics for the productive and fun atmosphere at the institute, even if I unfortunately did not get as much as I would have liked because of the corona-pandemic.

A big thanks goes to my parents who have supported me unconditionally throughout my studies and made this possible in the first place.

At last, I want so thank all my friends and great people around me who always had an open ear, when I was stressed or needed it for other reasons, and also for the great moments we shared. I would especially like to mention my sister, Maren, and my boyfriend, Daniel, who have certainly not always had an easy time with me in the last weeks and months but were always there.